

## **Two-Dimensional Joint Inversion of Radiomagnetotelluric and Direct Current Resistivity Data**

M. Emin Candansayar, Ankara University, Department of Geophysical Eng., 06100, Ankara, Turkey.  
E-mail:candansa@eng.ankara.edu.tr  
Bülent Tezkan, University of Cologne, Institute of Geophysics and Meteorology, Germany

---

### **SUMMARY**

A new algorithm for the 2D joint inversion of Radiomagnetotelluric (RMT) and Direct Current resistivity (DCR) data was developed. The algorithm uses finite difference technique to solve Helmholtz and Poisson equations for RMT and DCR methods, respectively. The regularized inversion with smoothness constrained stabilizer employed to invert the both data set. RMT method does not sensitive to resolve near surface resistivity blocks because of used limited frequencies. However, RMT data can be affected by small-scale near surface body which can cause static shift effect. RMT inversion sometimes generate blurred image because of near-surface small scale bodies. On the other hand, DCR method can resolve these near surface blocks. We inverted DCR and RMT data jointly and could resolve both near-surface and deeper structure.

We compared individual and joint inversion of synthetic RMT and DCR data and showed that the joint inversion result of synthetic data simulate the real model better than the individual inversion results of each method. We also tested our inversion algorithm on a field data set collected across an active fault in the test site, located close to the city of Kerpen in Germany. The preliminary inversion result of the field data also validated synthetic data inversion results.

**Keywords:** RMT, DCR, 2D Joint Inversion, synthetic data, field data

---

### **INTRODUCTION**

RMT and DCR methods are sensitive to subsurface electrical resistivity structure. RMT-method is an extension of the well-known Very-Low-Frequency (VLF) technique to higher frequencies. RMT uses radiotransmitters in a frequency range between 10 to 300 kHz. This method has been used with increasing popularity for different engineering applications (eg. Candansayar and Tezkan, 2006). On the other hand, DCR method is the most popular electrical methods that has also been used for different engineering problems. It is easy to collect DC sounding-profiling data by using the multi-electrode system. Nowadays, RMT and DCR data are generally interpreted by the help of 2D inversion algorithms.

The both methods are sensitive to the resistivity properties of the underground structures. Therefore, joint use of DCR and one of electromagnetic methods (e.g. Magnetotelluric, Transient Electromagnetic,

RMT) has long been used by many researchers (e.g. Sasaki, 1989) to reduce the ambiguity in interpretation. Harinarayana (1999) gave good review about the combined use of electromagnetic and DCR data. The 2D joint inversion of RMT and DCR data has not yet been published

In this study, we showed that the 2D joint inversion of synthetic and field RMT and DCR data give reliable results.

### **THE INVERSION ALGORITHM**

A new algorithm was developed in order to invert the RMT and DCR data jointly.

It is well known that, the inverse problem associated with electric and electromagnetic data is nonlinear and ill-posed. Therefore, it was generally solved by one regularization method. Here, we used smoothness-constrained least-squares approach (Tikhonov et al.,

1995). In this method, the minimization of objective function yields the normal equations,

$$(\mathbf{A}^T \mathbf{W}_d^T \mathbf{W}_d \mathbf{A} + \alpha \mathbf{C}^T \mathbf{C}) \Delta \mathbf{m} = \mathbf{A}^T \mathbf{W}_d^T \mathbf{W}_d \Delta \mathbf{d} - \alpha \mathbf{C}^T \mathbf{C} \mathbf{m}^{(k)} \quad (1)$$

where  $\mathbf{A}$  is the sensitivity (jacobian) matrix,  $\mathbf{m}^{(k)}$  is the model parameter vector at the  $k$ th iteration,  $\Delta \mathbf{d}$  is the vector of differences between the modeled response and the observed data,  $\Delta \mathbf{m}$  is the parameter correction vector to  $\mathbf{m}^{(k)}$ ,  $\mathbf{C}$  is a second-difference operator used to define the model roughness,  $\mathbf{W}_d$  is data weighting matrix consisting of the reciprocal of the data amplitude where data are assumed to have the same percentage standard deviation, and  $\alpha$  is regularization parameter. There is no unique approach for selecting  $\alpha$ . This value was selected as 2 after several trial for all data inversion presented in this paper. The solution of Eq. (1) for  $\Delta \mathbf{m}$  is equivalent to the least-squares solution of the rectangular system (Sasaki 2001),

$$\tilde{\mathbf{A}} \Delta \mathbf{m} = \tilde{\Delta \mathbf{d}} \quad (2)$$

where

$$\tilde{\mathbf{A}} = \begin{bmatrix} \mathbf{W}_d \mathbf{A} \\ \sqrt{\lambda} \mathbf{C} \end{bmatrix} \text{ and } \tilde{\Delta \mathbf{d}} = \begin{bmatrix} \mathbf{W}_d \Delta \mathbf{d} \\ -\sqrt{\lambda} \mathbf{C} \mathbf{m}^{(k)} \end{bmatrix}.$$

In the developed algorithm Eq.(2) solved by using QR factorization that gives fast result than SVD solution. The numerical solution obtained from Eq.(2) is known to be more accurate than the solution obtained via the normal Eq.(1) (e.g. Haber and Oldenburg, 2000). For joint inversion case of DCR and RMT data the  $\mathbf{A}$  and  $\Delta \mathbf{d}$  given as below

$$\mathbf{A} = \begin{bmatrix} \mathbf{W}_{dcr} \mathbf{A}_{dcr} \\ \mathbf{W}_{rmt} \mathbf{A}_{rmt} \end{bmatrix} \text{ and } \Delta \mathbf{d} = \begin{bmatrix} \Delta \mathbf{d}_{dcr} \\ \Delta \mathbf{d}_{rmt} \end{bmatrix}$$

where  $\mathbf{A}_{dcr}$ ,  $\mathbf{W}_{dcr}$  and  $\mathbf{A}_{rmt}$  and  $\mathbf{W}_{rmt}$ , sensitivity and weighting matrix for DCR and RMT, respectively. All elements of these two matrices,  $\mathbf{W}_{dcr}$  and  $\mathbf{W}_{rmt}$ , are equal to one. However, if we want to decrease effect of some data on some parameter, we change related element of the matrix between 0 and 1. In this paper, we decrease RMT data effect from solution of near surface block resistivity in joint inversion case.

Assuming the local electromagnetic fields as a plane wave (McNeill and Labson, 1991) and neglecting the displacement currents, magnetotelluric inversion algorithms can be used for RMT data interpretation (e.g. Candansayar and Tezkan, 2006). In our joint inversion algorithm, finite-difference forward solution

and partial derivative matrix calculation part was taken from the algorithm, R2DMTINV, developed by Candansayar(2002) for MT data inversion. On the other hand, Poisson equation was solved by using finite difference method according to Dey and Morrison (1978) and the partial derivative matrix was calculated according to Tripp et al.(1984) for DCR method. The forward solution of DCR data can be calculated for all possible classical configuration such as Wenner, Schlumberger, dipol-dipol, left- and right-side pole-dipol in the developed algorithm. Candansayar and Basokur(2001) showed that joint inversion of left- and right-side pole-dipole configurations (AMN and MNB) superior to any classical four-electrode configuration data inversion. We also used these two electrode configurations in our applications.

### INVERSION OF SYNTHETIC DATA

We first tested our inversion algorithm by using synthetic data. The synthetic data calculated for the dike model which is shown in Figure 1a. The model consists of two surface resistive body (1000 Ohm-m) and 30 Ohm-m conductive dike in a half-space of 100 Ohm-m.

Synthetic DCR data were calculated for 21 multi-electrode resistivity measurement systems for 10 levels (n) for this model. Distance between the each consecutive electrode (a) was selected as 5 meter. Totally 290 DCR data was obtained for left- and right-side pole-dipole configurations. Synthetic RMT data were also calculated for these 21 electrode locations for four frequencies, 234, 126, 53, 18.3 kHz yielding a total of 294 data, for both TE- and TM-mode apparent resistivities and impedance phase values. In all inversion run, homogenous half space is used as starting model with a resistivity of 110 Ohm-m.

The model mesh used in the inversion has 28 blocks in the x-direction and 14 blocks in the zdirection that yields totally 392 blocks. 2D inversion results of DCR and RMT data are shown in Figure 1.b and 1.c, respectively. The surface resistivity bodies can be acquired from the estimated model obtained from DCR data inversion whereas they can not be seen in the inversion result of RMT data. Skin depth range for 100 ohm-m homogenous medium for RMT frequencies used here is between 10m and 37m. This can be reason why RMT data inversion can not resolve these near surface resistive bodies. Note that, for all inversion result number of iteration and root mean squares (RMS) misfit are given on the top of each model.

On the other hand, the dike body can be better identified by the RMT inversion result than by the DCR inversion result. However, the joint inversion result resolved both near surface bodies and dike better

than individual inversion of DCR and RMT data (Figure 1.d). For a better resolution of the near surface structure DCR data was weighted in the joint inversion (Figure 1.d)

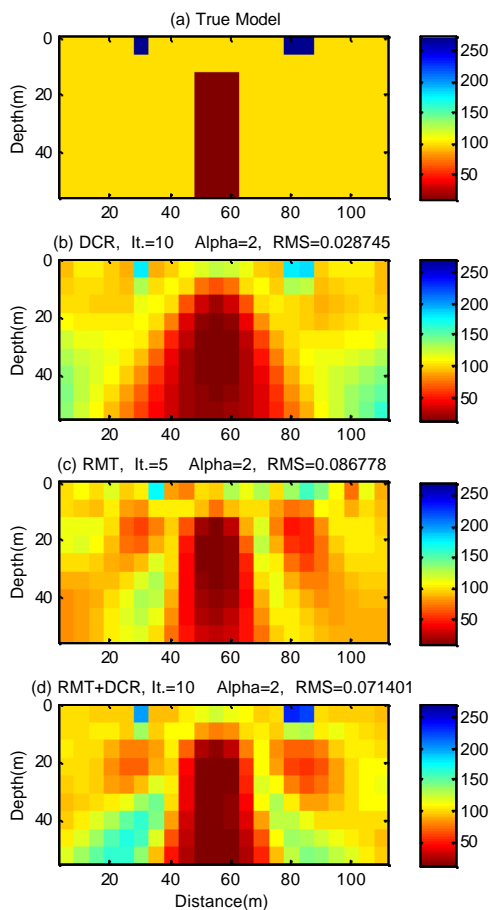


**Figure 1:** (a) Conductive dike model, (b) 2D inversion result of DCR data, (c) 2D inversion result of RMT data and (d) 2D joint inversion result of RMT and DCR data.

The fit between the inverted and calculated DCR data is shown in Figure 2 as pseudo-sections. The DCR data fit is acceptable. We also drawn inverted and calculated apparent resistivities and impedance phase curves both for TE- and TM-mode is shown in Figure 3. TE mode data fit is acceptable, whereas TM mode data fit is not well particularly for the stations close to resistive bodies at the surface.

### INVERSION OF FIELD DATA

The field RMT and DCR data are collected from Kerpen test site that located SW of the city of Kerpen, about 20 km west of Cologne, Germany. The

geological map indicates a minor, left-stepping, suspected fault traversing the site nearly at a North-South strike.

Our purpose in this survey was to detect the fault location and depth from the surface. We collect RMT data along 200 meter-long three parallel line that crossing the suspected fault. Distance between the each line was approximately 115 meter. The TE- and TM-mode apparent resistivity and impedance phase values in scalar mode collected for four frequencies, 234, 183, 75, 16.4 kHz, and for three frequencies, 198, 65.8, 12.1 kHz, respectively, on 25 stations, that yields 350 data. The distance between each consecutive station was 10 m. The expected boundary of the fault was densely sampled (with station interval of 5m). The DCR data also collected along the same three parallel lines by using ABEM SAS 1000 imaging system with 41 electrodes. The DCR data were collected for two different electrode separations by using left- and right-side pole-dipole configurations. The first, distance between the each consecutive electrode was selected 5 meter and the data were collected for fixed distance between the potential electrode ( $MN=a=5$  meter) and for 10 level ( $n=1,3,\dots,19$ ). The second, between the -50 and 50 meters along the line direction, the distance between the each consecutive electrode were selected as 2.5 meter and the data were collected for fixed distance between the potential electrode ( $MN=a=2.5$  meter) and for 5 level ( $n=1,2,\dots,5$ ) to get more detailed information from the near surface resistivity structure around the suspected fault.

Here, we only presented preliminary 2D inversion result of the RMT and DCR data collected along line 2. DCR data that collected by using the first field setup, inversion result is shown in Figure 4a. Here we can acquire two layers and also a fault trace between 20 and 40 meter on line direction. However, we can acquire three layers from RMT data inversion (Figure 3b). The fault trace can also be distinguished from RMT estimated model but not as clear as DCR data inversion.

Finally we inverted RMT and DCR data jointly (Fig 4.c). In the estimated model we can distinguish the fault trace more accurate than individual inversion result of RMT and DCR data. The fit between the measured and calculated DCR and RMT data are shown in Figure 5 and 6, respectively.

### CONCLUSIONS

We have developed a new 2D joint inversion algorithm for RMT and DCR data. Synthetic data inversion result showed that small-scale near-surface body can not be acquired from RMT inversion result.

However, RMT data can be affected by small-scale near surface body which can cause static shift effect. RMT inversion sometimes generate blurred image because of near-surface small scale bodies. On the other hand, DCR method can resolve these near surface blocks. We inverted DCR and RMT data jointly and resolve both near-surface and deeper structure.

#### ACKNOWLEDGEMENTS

M.E.Candansayar was granted postdoctoral fellowships by TÜBİTAK (Scientific and Technical Research Council of Turkey) and DFG (Deutsche Forschungsgemeinschaft). This work was done under the TÜBİTAK Project No. ÇAYDAG 104Y073.

#### REFERENCES

- Candansayar, M.E., 2002. Regularized inversion of magnetotelluric data by consecutive use of conjugate gradient and least-squares SVD solvers. PhD. Thesis, Ankara University, Turkey.
- Candansayar M.E. and Basokur A.T. 2001. Detecting small-scale targets by the 2D inversion of two-sided three-electrode data: application to an archaeological survey. *Geophysical Prospecting* 49, 13–25.
- Candansayar M.E. and Tezkan B., 2006. A comparison of different radiomagnetotelluric data inversion methods for buried waste sites. *Journal of Applied Geophysics*, 58, 218-231.
- Dey, A. and Morrison, H. F. 1978. Resistivity modelling for arbitrarily shaped two-dimensional structures. *Geophysical Prospecting*, 27, 106-136.
- Haber, E. and Oldenburg, D., 2000. *Computational Geosciences*, 4, 41-63.
- Harinarayana, T., 1999. Combination of EM and DC measurement for upper crustal studies. *Surveys in Geophysics*, 20, 257-278.
- McNeill, J.D. and Labson, V., 1991. Geological Mapping Using VLF Radio Fields, in *Electromagnetic Methods in Applied Geophysics*, Editor. M.N. Nabighan., Chapter 7, 521-640. Soc. Expl.Geophys. publication.
- Sasaki, Y., 2001. Full 3-D inversion of electromagnetic data on PC. *Journal of Applied Geophysics*, 46, 45-54.
- Sasaki, Y., 1989. Two-dimensional joint inversion of MT and dipole-dipole resistivity data. *Geophysics*, 54, 254-262.
- Tikhonov, A.N., Goncharky, A.V., Stepanov, V.V., and Yagola, A.G. 1995. Numerical methods for the solution of ill-posed problems. Kluwer Academic Publishers.
- Tripp, A.C., Hohmann, G.W., and Swift, C.M., 1984. Two-dimensional resistivity inversion. *Geophysics*, 49, 1708-1717.

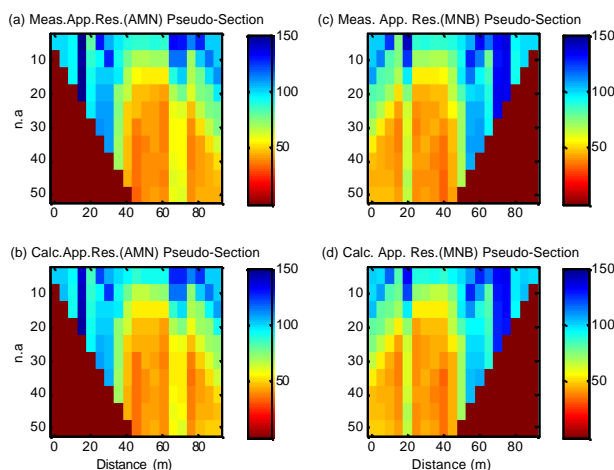


**Figure 2:** Measured apparent resistivity pseudo-sections for (a) AMN and (b) MNB configurations. Calculated apparent resistivity pseudo-sections for (a) AMN and (b) MNB configurations obtained from 2D joint inversion result (Fig.1d).

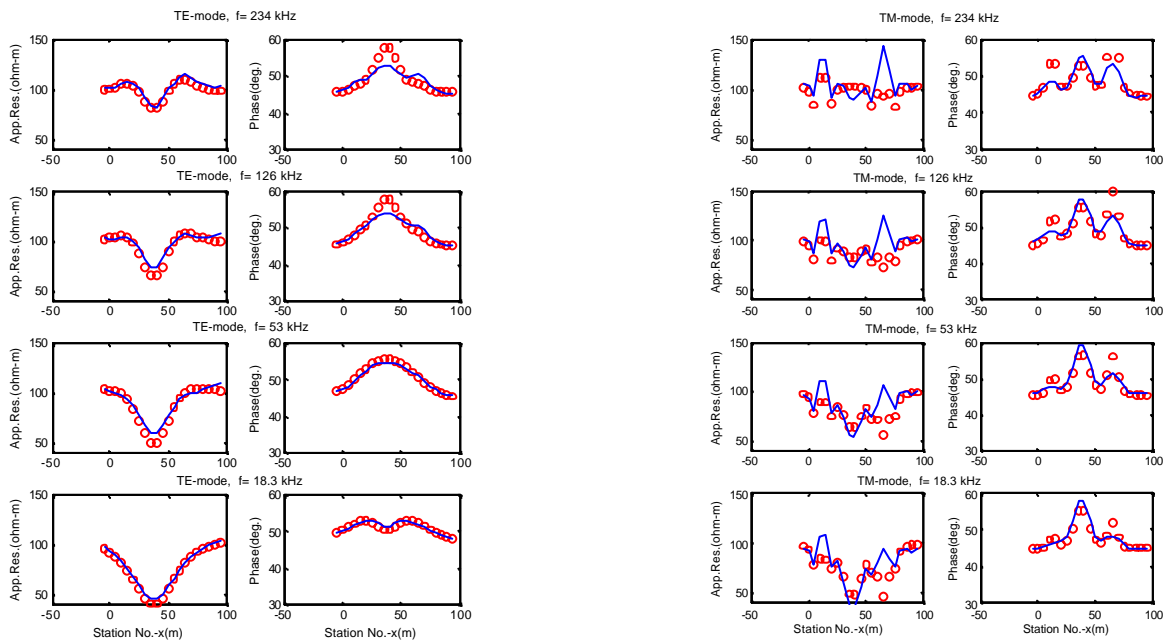


**Figure 3:** Comparison between measured and calculated data for TE- and TM-mode from the estimated model shown in Fig. 1d, on left and right panel, respectively, obtained from 2D joint inversion result (Fig. 1d). The circular shape symbols mark the observed data and the solid line marks the calculated data.

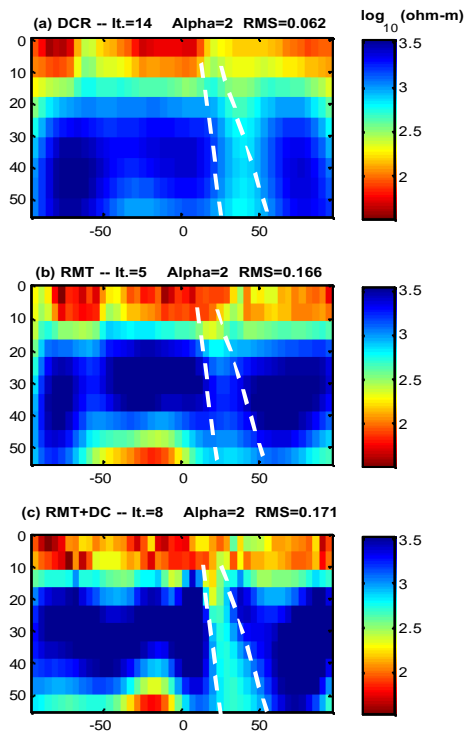


**Figure 4:** Estimated model obtained from 2D inversion of (a) DCR data, (b) RMT data and 2D joint inversion result of (c) RMT and DCR data. The data set collected from Kerpen test site, Germany. The white colored dashed lines show the expected fault location.

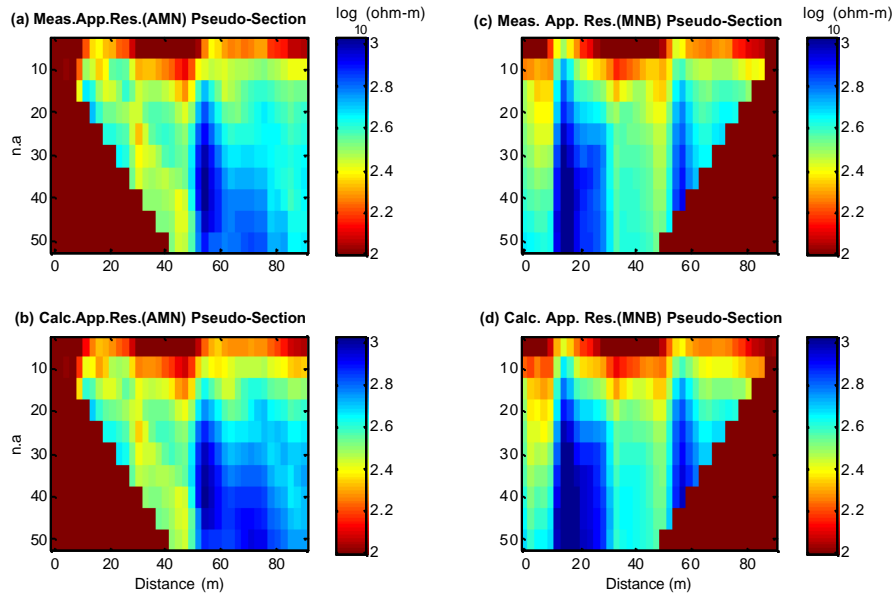


**Figure 5:** Measured apparent resistivity pseudo-sections for (a) AMN and (b) MNB configurations. Calculated apparent resistivity pseudo-sections for (a) AMN and (b) MNB configurations obtained from 2D joint inversion result (Fig.4c).

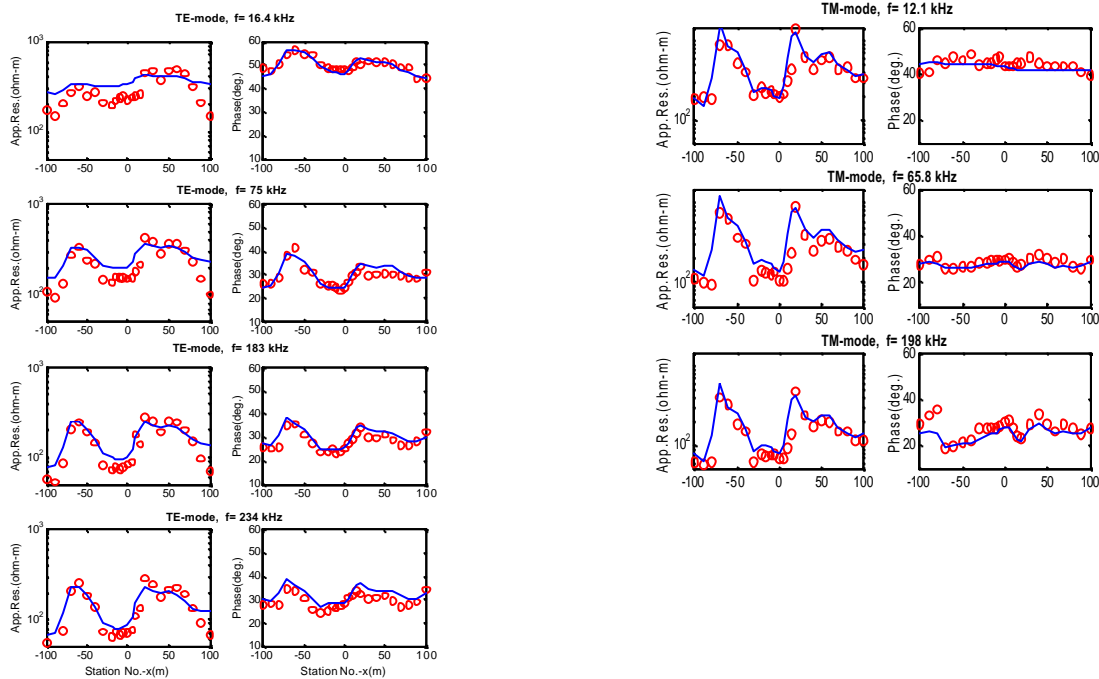


**Figure 6:** Comparison between measured and calculated data for TE- and TM-mode from the estimated model shown in Fig.1d, on left and right panel, respectively, obtained from 2D joint inversion result (Fig.4c). The circular shape symbols mark the observed data and the solid line marks the calculated data.

## A structural approach to joint three-dimensional inversion of geophysical data

Niklas Linde, Université Paul Cezanne, CNRS-CEREGE, Aix-en-Provence, France  
Ari Tryggvason, Uppsala Universitet, Department of Earth Sciences, Uppsala, Sweden  
Andrew Binley, Department of Environmental Science, Lancaster University, Lancaster, UK.  
Laust B. Pedersen, Uppsala Universitet, Department of Earth Sciences, Uppsala, Sweden  
André Revil, Université Paul Cezanne, CNRS-CEREGE, Aix-en-Provence, France

---

### SUMMARY

Structural approaches to joint inversion, where structural similarity between different geophysical models are minimized, provide a fundamental improvement in our ability to jointly invert disparate data sets (Haber and Oldenburg, 1997; Gallardo and Meju, 2003). Two-dimensional applications include dc resistivity, controlled source audio-magnetotellurics, and seismic refraction data. In this work we report on recent applications to three-dimensional problems, namely to synthetic local earthquake tomography with joint inversion for P- and S-wave velocities (Tryggvason and Linde, 2006) and crosshole electrical resistance tomography and ground penetrating radar traveltimes collected in unsaturated sandstone for joint inversion of electrical conductivity and relative permittivity (Linde et al., 2006). We also report on a new method to calculate stochastic regularization operators that are based on a given stationary geostatistical model. Stochastic regularization operators provide a means to incorporate *a priori* information about the spatial variability of the model property of interest and to test the influence of the regularization applied. We suggest that a structural approach to joint inversion could be useful to jointly invert EM and seismic data once 3D inversion of EM data can be performed within reasonable computational times.

In addition to its flexibility, we believe that the major advantage of the structural approach to joint inversion is that space-varying petrophysical relationships are obtained without imposing any rock physics models. The resulting petrophysical relationships may make it possible to understand features of the system under study that could not be resolved by using only one geophysical method or a combination of geophysical methods that were inverted individually.

**Keywords:** Joint inversion, stochastic regularization, and rock physics

---

### INTRODUCTION

A structural approach to joint inversion has recently been applied to jointly invert different geophysical data sets at both local and regional scales. A major advantage with the structural approach is that no functional relationships between different physical properties must be defined. Most physical properties that we invert for in geophysics are dependent on several rock properties and associated state variables, e.g., a high electrical conductivity anomaly might be explained by either saline groundwater, clay minerals, or partial melts. This means that calibrated petrophysical relationships are likely to break down away from calibration points and that most theoretical

rock physics models are likely to be either under-determined or too simplified to allow joint inversion of geophysical data using functional relationships.

### A STRUCTURAL APPROACH TO JOINT INVERSION

Haber and Oldenburg (1997) jointly inverted synthetic gravity and seismic tomography data in 2D by assuming that major changes in the model properties occur at the same location. The problems with their method are that the directional dependence of the change is neglected and thresholds that define what constitute a large change need to be defined. Gallardo and Meju (2003) solved these problems by introducing

the cross-gradients function to quantify structural similarity between two models  $\mathbf{m}^A$  and  $\mathbf{m}^B$  as

$$\mathbf{t}_p = \nabla \mathbf{m}_p^A \times \nabla \mathbf{m}_p^B. \quad (1)$$

If the cross-gradients function is zero at a point in space, it implies that the gradients of the two model properties point in the same or opposite direction, or that the gradients of one of the models are zero. The discretized formulation of the cross-gradients function using a forward difference scheme is given here for the  $x$ -direction

$$\begin{aligned} t_p^x(i,j,k) = & \frac{1}{\Delta y \Delta z} \left( m^A(i,j+1,k) - m^A(i,j,k) \right) \\ & \left( m^B(i,j,k+1) - m^B(i,j,k) \right) + \\ & - \frac{1}{\Delta y \Delta z} \left( m^A(i,j,k+1) - m^A(i,j,k) \right) \\ & \left( m^B(i,j+1,k) - m^B(i,j,k) \right), \end{aligned} \quad (2)$$

where the indices  $i$ ,  $j$ , and  $k$  define the model parameters in the  $x$ -,  $y$ -, and  $z$ -directions, respectively;  $\Delta x$ ,  $\Delta y$ , and  $\Delta z$  are the model discretization distances. The cross-gradients function for the present iteration is estimated by a first order Taylor expansion around the cross-gradients function at the previous iteration, shown here for

$$\mathbf{t}_{p+1}^x \cong \mathbf{t}_p^x + \mathbf{B}_p^x \begin{pmatrix} \mathbf{m}_{p+1}^A - \mathbf{m}_p^A \\ \mathbf{m}_{p+1}^B - \mathbf{m}_p^B \end{pmatrix}, \quad (3)$$

where  $\mathbf{B}_p^x$  is the Jacobian of the cross-gradients function in the  $x$ -direction. Every row of  $\mathbf{B}_p^x$  has six non-zero elements that can easily be derived from equations (2).

Gallardo and Meju (2003, 2004) developed a 2D inversion method to jointly invert dc resistivity and seismic refraction data where Lagrange Multipliers were used to keep the cross-gradients function close to zero. Gallardo (2005) also applied this joint inversion method to Controlled Source Audio Magneto-tellurics (CSAMT) and seismic refraction data. Gallardo et al. (2005) introduced a different solution strategy that was based on quadratic programming. However, neither Lagrange multipliers nor quadratic programming are suitable for 3D inversion because the necessary memory allocations are prohibitive for most problems.

However, iterative methods such as LSQR (Paige and Saunders, 1982) are well suited for 3D inversion problems, especially if the sparseness of the matrix system to solve for is utilized.

## A structural approach in three dimensions

There have been two reported applications of joint inversion based on a structural approach in 3D, where the LSQR method was used in both cases.

Tryggvason and Linde (2006) applied the cross-gradients function as an additional constraint to a synthetic local earthquake (LE) tomography experiment with joint inversion for P- and S-wave velocities. The reported benefits compared with damping around a given Vp/Vs-ratio were that (1) the magnitudes of the Vp/Vs-anomalies were better resolved, (2) that no Vp/Vs-ratio needed to be assumed, and (3) that the magnitude of the Vp/Vs-anomalies were well resolved even if the data set were depleted in S-wave travel times.

Linde et al. (2006) used the cross-gradients function to jointly invert crosshole electrical resistance tomography (ERT) and crosshole ground penetrating radar (GPR) traveltimes collected between eight different boreholes in unsaturated sandstone. The jointly inverted models allowed an improved hydrological zonation. Rock physics models were used together with scatter plots between relative permittivity and electrical conductivity to estimate water content, the electrical formation factor, and the surface conductivity of each zone. These estimates were in good qualitative agreement with both borehole logs and available core samples. Note that no estimates of surface conductivity could have been obtained from only one of the methods. Linde et al. (2006) also introduced a new method to calculate stochastic regularization operators (see next section) that are based on an underlying geostatistical model of the electrical conductivity and relative permittivity. The geostatistical models were determined based on EM conductivity logs collected in the boreholes, zero-offset GPR profiles, and geological understanding.

## Stochastic regularization operators

Regularization that penalize roughness give models with strong spatial correlations and regularization that penalize deviations from an *a priori* model give models that are close to an initial model, but with no spatial correlation. Maurer et al. (1998) showed that regularization of inverse problems based on a stochastic regularization operator,  $\mathbf{C}_m^{-0.5}$ , can be expressed as a combination of smoothness and damping regularization operators, resulting in geologically more reasonable models that are consistent with geostatistical descriptions of geological media.

There are conditions under which  $\mathbf{C}_m^{-0.5}$  can be calculated efficiently. The model covariance matrix,

$C_m$  is a symmetrical Toeplitz matrix if the correlation function is stationary and the grid discretization is uniform in each direction (e.g., Dietrich and Newsam, 1997). We used circulant embedding and the diagonalization theorem for circulant matrices to compute the stochastic regularization operator,  $C_m^{-0.5}$ , in a computationally efficient way. We can solve for the first column of  $C_m^{-0.5}$  and all other columns of  $C_m^{-0.5}$  can be calculated by shifting the first column circularly, i.e., such that the last element becomes first and all other elements are shifted forward by one. The resulting regularization operator is sparse for most inverse problems and the associated memory requirements are typically a few times larger compared with storing the roughness matrix. The stochastic regularization operator not only allows incorporation of *a priori* assumptions regarding the spatial characteristics of the physical property of interest, but it also allows the modeler to evaluate the influence of the regularization by performing repeated inversions with different regularization operators.

### Three-dimensional inversion schemes that include plane-wave EM data?

Three-dimensional inversion of RMT, CSAMT, or MT data are computationally demanding, but new inversion codes (e.g., Siripunvaraporn et al., 2005) will hopefully make it possible to routinely perform three-dimensional inversion of MT data in the coming years. The computational costs of our structural approach to joint inversion are mainly tied to the calculation of the Jacobian and the LSQR algorithm, whereas memory requirements are mainly determined by the size of the Jacobian. Therefore, only a small computational overhead would occur if, for example, LE tomography data were jointly inverted with CSAMT data compared with inverting the CSAMT data only. Likewise, the memory requirements would not increase significantly if both the P- and S-wave data were included to allow joint inversion of three different data types. One potential application could be to jointly invert P- and S-wave traveltime data with CSAMT data collected over geothermal or seismologically active regions.

### CONCLUSIONS

A structural approach to joint inversion where structural similarity between two models is quantified with the cross-gradients function has successfully been applied to jointly invert data collected with diverse geophysical methods. Its success can be attributed to its flexibility and the weak underlying assumptions. We propose that a structural approach could be useful in MT studies as well, especially when 3D inversion of MT data can be performed within reasonable computation times. The structural approach has the

advantage that no petrophysical relationship needs to be defined *a priori*—even though a known correlation coefficient could be included in the model covariance matrix—but is instead obtained *a posteriori*.

Joint inversion schemes based on the cross-gradients function are likely to converge to the target misfit given that it can be reached for the individual inversions. However, this does not necessarily imply that a useful model has been found and that the resulting petrophysical relationships are close to the underlying petrophysical relationships. The reason for this is simply that regularization is still needed—albeit less than for the corresponding individual inversions—to converge to a unique solution. Furthermore, the validity of minimizing the cross-gradients function must be carefully assessed for each application by using rock physics models and understanding of the underlying geology.

Another concern is related to differences in resolution and spatial coverage of the geophysical data types that are jointly inverted. For example, a given impedance tensor has some sensitivity to the electrical conductivity at each model element, whereas a seismic wave if modeled as an infinitely thin ray is only sensitive to the few model pixels that the ray crosses on its perceived travel to the receiver. In this case, regularization that is based on damping is likely to decouple the joint inversion for electrical conductivity and seismic velocity. Stochastic regularization operators, on the other hand, ensure interpolation within the model at a scale the modeler find appropriate.

### REFERENCES

- Dietrich, C.R., and Newsam, G.N., 1997, Fast and exact simulation of stationary Gaussian processes through circulant embedding of the covariance matrix. *SIAM Journal on Scientific Computing*, 18(4), 1088-1107.
- Gallardo, L.A., and Meju, M.A., 2003, Characterization of heterogeneous near-surface materials by joint 2D inversion of dc resistivity and seismic data. *Geophysical Research Letters*, 30(13), 1658, doi:10.1029/2003GL017370.
- Gallardo, L.A., and Meju, M.A., 2004, Joint two-dimensional DC resistivity and seismic travel time inversion with cross-gradient constraints. *Journal of Geophysical Research*, 109, B03311, doi: 10.1029/2003JB002716.
- Gallardo, L. A., 2005, Joint Two-dimensional inversion of geoelectromagnetic and seismic refraction data with

---

cross-gradients constraint. PhD dissertation, Lancaster University, Lancaster, UK.

Gallardo, L.A., Meju, M.A. and Pérez-Flores, M.A., 2005, A quadratic programming approach for joint image reconstruction: mathematical and geophysical examples. *Inverse problems*, 21(2), 435-452.

Haber E, and Oldenburg, D., 1997, Joint inversion: A structural approach. *Inverse problems*, 13(1), 63-77.

Linde, N., Binley, A. Tryggvason, A., Pedersen, L.B., and Revil, A. 2006, Improved hydrogeophysical characterization using joint inversion of crosshole electrical resistance and ground penetrating radar traveltimes data. submitted to *Water Resources Research*.

Maurer, H., Holliger, K. and Boerner, D.E., 1998, Stochastic regularization: Smoothness or similarity?. *Geophysical Research Letters*, 25(15), 2889-2892.

Paige, C.C., and Saunders, M.A., 1982, LSQR: An algorithm for sparse linear equations and sparse least squares. *ACM Transactions on Mathematical Software*, 8(1), 43-71.

Siripunvaraporn, W., Egbert, G., Lenbury, Y. Uyeshima, M., 2005, Three-dimensional magnetotelluric inversion: data-space method, *Physics of the Earth and Planetary Interiors*. 150(1-3), 3-14.

Tryggvason, A., and Linde, N. 2006, Local earthquake (LE) tomography with joint inversion for P- and S-wave velocities using structural constraints. *Geophysical Research Letters*, 33, L07303, doi:10.1029/2005GL025485.

## **Application of Electrical Resistivity and Transient Electromagnetic for Evaluation Sea water intrusion at Fan of Wadi Feiran, Sinai, Egypt**

EL-Said A. EL-Sayed, National Research Institute of Astronomy and Geophysics, 11722 Helwan, Cairo,  
Egypt.

---

### **SUMMARY**

The fan of Wadi Feiran at the south western part of Sinai, Egypt overlooking at the Gulf of Suez is very talented area for Oil industry and agricultural activities. The study area suffers extreme arid conditions with long, hot, rainless summers and mild winters. So it depends on underground water in its agricultural activities. Quaternary aquifer in the plan area has suitable thickness to use as the main water source for different purposes. Due to the presence of this aquifer in contact with the sea water of the Gulf of Suez, the fresh water is contaminated mainly in the coastal part and to different extensions to the eastern side. The present study is concerning with the application of surface geophysical techniques to study the spreading out of sea water intrusion and put forward the suitable locations for futures digging wells. One-dimensional numerical inversion of individual ER and TDEM sounding data capitulate the resistivity of the aquifer materials beneath each survey point. However, the ambiguity in soundings interpretation arises from the principle of equivalence leading to massive miss-interpretation. 2-D resistivity tomography in addition to joint inversion of ER and TDEM can greatly enhance the results of processing and achieve the aim of study. From the results of interpretation of the electrical resistivity, time domain electromagnetic and 2-D resistivity tomography data are represented to the area of study is concerning three geoelectrical layers. The first geoelectrical layer is represented by alluvial and gravels deposits. The second layer with low resistivity is represented as clayey sand which is saturated by sea water. The third layer is sandy clay with higher resistivity than the second layer. The sea water intrusion is very appear along the profile parallel to the shore line of the Gulf and extended in the east direction towards the Wadi Feiran.

**Keywords:** : DC resistivity, TEM, groundwater

---

### **INTRODUCTION**

In many developed and developing countries there is not only a heavy reliance on ground water as a primary drinking supply but also as a supply of water for both agricultural and industrial use. Among these interesting areas in Egypt, is the fan of Wadi Feiran at the south-western side of Sinai, overlooking at the Gulf of Suez. Geophysics, especially geoelectric techniques have been successfully used to detect the fresh water/salt-water interface in coastal aquifers (Barker, 1980). These methods are including the dc resistivity method and transient electromagnetic induction (TEM) method (Stewart, 1982) Resistivity surveys are often used to search for ground water in both porous and fissured media. These methods provide detailed information about the geometry, source and amount of contamination.

In areas where the ground water is significantly saline, the aquifer resistivity is reduced considerably and resistivity method can delineate the boundaries of the body of saline water. Griffith and Barker (1993) present the results of strong resistivity contrast, which can occur across the junction between fresh and saline water using the resistivity survey. Additionally, large differences between the resistivity of saltwater saturated zones and freshwater saturated zones have been used by a number of investigators for determination of saltwater intrusion in many coastal areas (e.g. Frohlich et al., 1994).

The study area is located between latitudes 33° 12' and 33° 18' E and longitude of 28° 39' to 28° 46' N (Fig.1). This work represents an attempt to study the subsurface structural setting and delineate the ground water aquifer in the Fan of Wadi Feiran area, as well as mapping the seawater intrusion in the fresh water aquifer is performed.

## GEOMORPHOLOGICAL AND GEOLOGICAL CONTEXT

The area of study is represented as small portion of the rugged mountainous belt of South Sinai, which consists of igneous and metamorphic rocks. The study area suffers extreme arid conditions with long, hot, rainless summers and mild winters. The area is temporary floods and dissected with numerous wadis which drain the surrounding high mountains and flow towards the Gulf of Sues. Wadi Feiran is one of the most important basins in the Southwestern Sinai. The channel of wadi feiran and its tributaries are filled by alluvium and lacustrine deposits forming reasonable reservoir for groundwater accumulation.

From the geological point of view, the study area is occupied by deformed Precambrian igneous and metamorphic rocks consisting mainly of gneisses and granites. In such a mountainous area, a well stratified lacustrine sandy and pebbly deposits fill the main wadis. Overlying these sediments Quaternary alluvium deposits form the relatively thin vineer covering the floor of main wadis and plains (Said, 1962). The main succession of the area of study is classified into dry wadi fill, saturated wadi fill, saturated basement rocks and crystalline basement rocks.

## GEOPHYSICAL DATA

Surface geophysical methods vary widely in the terms of the parameters they measure, including physical and chemical parameters. Some methods are best used as an effective means of measuring lateral changes, (e.g. resistivity profiling and, spontaneous potential). Others are best used for measuring depth and thickness of geologic strata, (e.g. resistivity sounding and time domain electromagnetic). In most cases, measurements will be made on a station by station along profiles. However; some methods can provide continuous measurements along a profile line, which is called tomography (Dahlin, 1996). These continuous measurements provide high lateral resolution for mapping subtle lateral changes in subsurface conditions. In this study we have experimented the time domain electromagnetic, DC resistivity soundings and DC resistivity tomography surveys.

### Time domain electromagnetic data

Electromagnetic techniques have been extensively developed and adapted over the last few years to map lateral and vertical conductivity changes of the shallow subsurface (Fitterman and Stewart, 1986; McNeill, 1990). While the final output is similar to that from electrical techniques, several advantages with the electromagnetic techniques result in an increased resolution and more cost-effective application. Time domain electromagnetic technique has been applied in

this study to measure the electrical conductivity (or resistivity) of the subsurface succession by inducing pulsating currents in the ground via a transmitter coil. After abruptly terminating the current, a receiver coil measures the decaying of electromagnetic field over a number of fixed times. The method is extensively discussed by Kaufman and Keller (1983), McNeill (1990) and Nabighian, (1991). Many regional case histories are now available to demonstrate the utility of TDEM for instance, Fitterman and Stewart, (1986) and Nabighian, (1991).

Using the SIROTEM III acquisition system (Buselli and O'Neill, 1977), suite of numbers of 19 TDEM measurements were made at different stations and distributed in the area of study as shown in figure(1) in the form of tow profiles. One of them is measured parallel to shoreline of the Gulf and the other is perpendicular towards the eastern side. A simple coincident loop configuration was employed (Fitterman and Stewart, 1986) with side length of 100 m and composite recording mode.

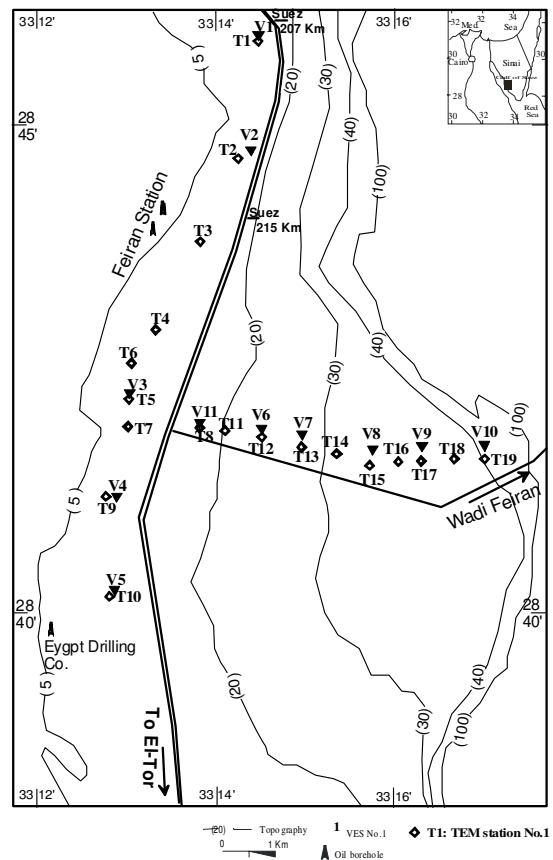


Figure 1. Location map of the study area.

### Geoelectrical resistivity sounding

The use of electrical resistivity measurements has been a favorite tool of geophysicists because of the wide range of resistivity values found in nature which represents a greater dynamic range for this technique

than most other commonly used methods. The resistivity soundings conducted in this work concerns with a DC resistivity survey utilizing the well-known Schlumberger array. The measurements are performed along the same two profiles which achieved in the TDEM measurements. Eleven vertical electrical soundings (VESes) were measured as shown in figure (1) with current electrode separation (AB) varying from 1 m up to 1000 m in successive steps. The increase of potential electrode spacing is often marked by a discontinuity in the field curve. At the discontinuities, we repeated the measurements, and then the field curves are smoothed before digitization. Figures (2) and (3) are illustrating the 1-D cross sections resulting from the interpretation of the resistivity and electromagnetic data respectively. From the description of these two cross sections, the area of study is concerning of three geoelectrical layers. The first geoelectrical layer is represented by alluvial and gravels deposits. The second layer with low resistivity is represented as clayey sand which is saturated by sea water. The third layer is sandy clay with higher resistivity than the second layer. The same data set had been inverted in 2-D, using Uchida, (1991) technique. Figure (4) illustrates the 2-D geoelectrical cross section along the same profiles. The 2-D cross section shows the good agreement with the results of 1-D cross section while elucidating more details

### Geoelectrical resistivity profiling

The advent of fast computing technologies permitted a broad use of the electrical resistivity tomography for environmental purposes (Dahlin 1996; LaBrecque et al. 1996; Oldenburg and Li, 1999). In electrical resistivity tomography applications, the current is introduced into the ground through one pair of electrodes. A second pair of electrodes is then used to quantitatively measure the voltage pattern on the surface resulting from the current flow pattern of the first set of electrodes. If multiple electrodes are used and the data are recorded automatically, the surveyed area can be searched more efficiently and various depths can be examined at the same time.

In this work, resistivity data were acquired along four profiles, (Fig. 1), using the electrical tomography method with dipole-dipole array of a maximum N (ratio of maximum and minimum electrode spacing) that equals to 8. The data collection was performed using the SYSCAL-R2 resistivity meter of (IRIS, 1998). Usually, the apparent resistivity pseudo section produces a distorted image of the subsurface resistivity. Hence, inversion of the field observations is the standard procedure to obtain an estimate of the true resistivity distribution. A fast numerical approach is then used to optimize an initial multilayer model constructed directly from the observed apparent

resistivity values (Loke, 2002). A finite difference or finite element technique is usually used to calculate the 2-D forward response of the model. By the subsequent iterations, the model is updated until an acceptable rms misfit between the observed and model pseudo section is achieved. Figure (5) illustrates the resistivity cross section along the LINE-3. The results of 2-D profiling are giving the same results of the 1-D of the resistivity and Transient electromagnetic and 2-D inversion but with less depth and detailed information of the shallow section.

### DISCUSSION AND CONCLUSION

The area of study is concerning three geoelectrical layers. The first geoelectrical layer is represented by alluvial and gravels deposits. The second layer with low resistivity is represented as clayey sand which is saturated by sea water. The third layer is sandy clay with higher resistivity than the second layer.

The interface of sea water intrusion is clearly observed in profile (2), which is perpendicular to the shore line as shown in figures (2 and 3). The interface is separate between shallow clay, high resistive wadi fill deposits and very low resistivity of sea water.

The depth to the seawater interface ranges from 10m near to the sea at VES No. 3 to 60 m. at VES No. 10 along the profile (2) as shown figure (2). This depth is abruptly increased at VESes Nos. 9 and 10. This increasing may be attributed to the affecting of high pumping rate in the well field of Wadi Feiran. This assumption is supported by the observation. That, the depth to water in Wadi Feiran is more or less the same as the depth in VESes 9, and 10 in profile (2). According to this hypothesis, the ground water in Wadi Feiran should be affected by sea water. It is recommended to carry out a geochemical study to investigate this phenomenon.

### REFERENCES

- Barker R.D, 1980: Application of Geophysics in groundwater investigations. *Water Surv.*, 84, 489-492.
- Buselli, G., and O'Neill, B, 1977. SIROTEM: a new portable instrument for multichannel transient electromagnetic measurements. *Bull. Austral. Soc. Expl. Geophys.* 8, 82-87.
- Dahlin, T., 1996. 2D resistivity surveying for environmental and engineering applications: *First Break* 14, 275-283.
- Fitterman, D.V. and Stewart, M., 1986. Transient electromagnetic sounding for groundwater. *Geophysics* 54, 995-1005.
- Frohlich, R.K., Urish, D, Fuller, J and Reilly M.O., 1994: use of geoelectrical methods in groundwater

pollution surveys in a coastal environment. *J. Applied Geophysics* 32, 139-154.

Griffiths, D.H and Barker, 1993: Two-dimensional resistivity imaging and modelling in areas of complex geology. *J. Appl. Geophysics.* 29, 211-226

IRIS-Instruments, 1998. User manual of Syscal Junir-R2, Multi- electrode system. Orleans Cedex, 98 p.

Kaufman, A., and Keller, G., 1983. Frequency and transient soundings. Elsevier science pub. Inc.

Kelly, W., 1976: Geoelectric sounding for delineating groundwater contamination. *Ground water*, 14, pp. 6-10.

LaBrecque, D., Ramirez, A., Daily, W., Binley, A., and Schima, A. 1996. ERT Monitoring of Environmental Remediation Processes. *Measurement Science and Technology* 7, 375-383.

Loke, M. H., 2002. Tutorial: 2-D and 3-D electrical imaging surveys. Penang, Malaysia, University of Sains Malaysia, Unpublished training Course lecture notes.

McNeill, J., 1990. Use of electromagnetic methods for groundwater studies. In: Ward, S.H. (Ed.). *Geotechnical*

and environmental geophysics, v.1: Review and Tutorial, Society of Exploration Geophysicists Investigations No. 5, 107-112.

Nabighian, M., 1991. *Electromagnetic Methods in Applied Geophysics - Applications part A and B.* Society of Exploration Geophysicists, Tulsa.

Oldenburg, D. W., and Li, Y. G., 1999. Estimating depth of investigation in dc resistivity and IP surveys. *Geophysics* 64, 403-416.

Said, R., 1962, *The geology of Egypt.* Elsevier, Amsterdam-New York, 377pp.

Said, R., 1990, *Geology of Egypt,* Balkema Pub. Rotterdam, Netherlands, 734pp.

Stewart M.T., 1982: Evaluation of electromagnetic methods for rapid mapping of salt water interfaces in coastal aquifers. *Groundwater*, 20,538-545.

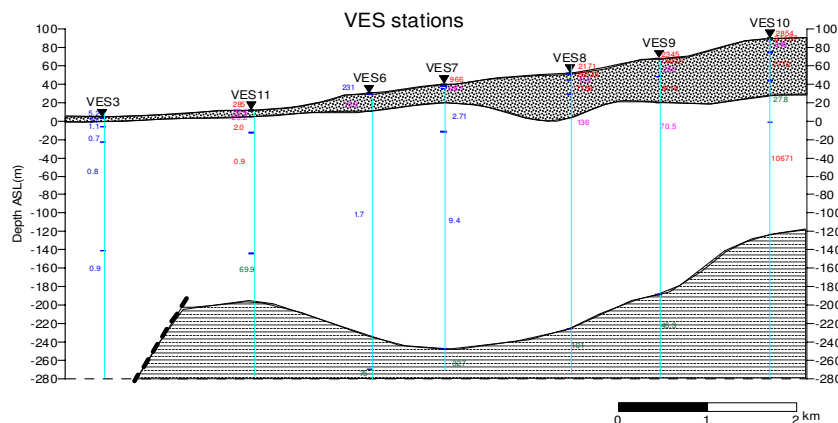


Figure 2. The geoelectrical cross section results from 1-D VES interpretation along profile 2.

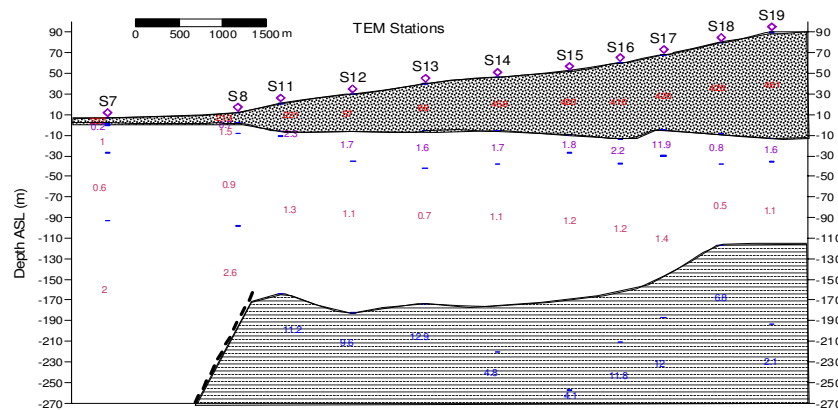


Figure 3. The geoelectrical cross section results from 1-D TEM interpretation along profile 2.

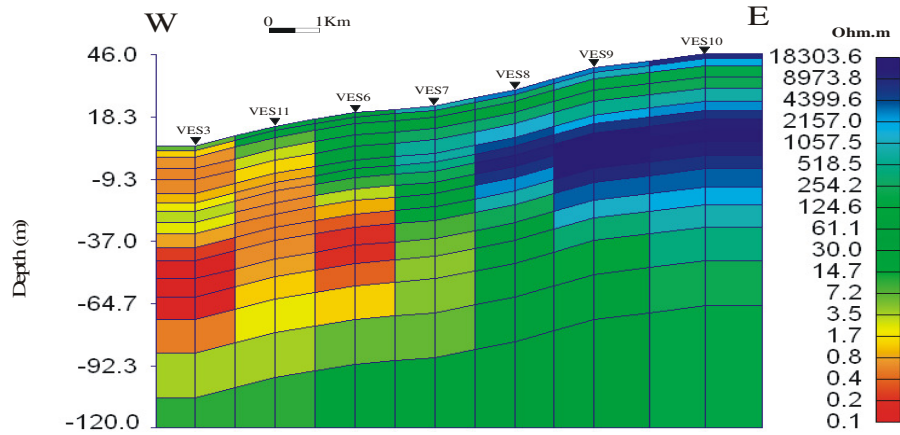


Figure 4. The geoelectrical cross section resulted from 2-D VES interpretation along profile 2.

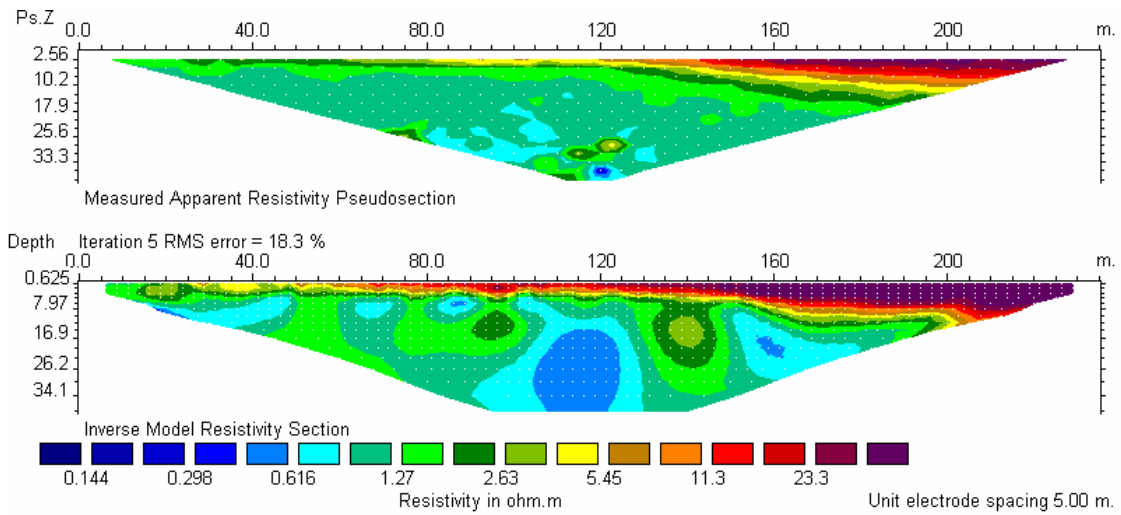


Figure 5. The geoelectrical cross section resulted from 2-D resistivity profiling along Line 1.

## Joint 2D audiofrequency magnetotelluric and seismic refraction cross-gradients imaging: implications for lithofacies and structural classification

Max A. Meju, Department of Environmental Science, Lancaster University, Lancaster LA1 4YQ, UK  
 Luis A. Gallardo, Earth Science Division, CICESE, Mexico

---

### SUMMARY

We have applied a recently developed 2D joint cross-gradients inversion approach to collocated high resolution audiomagnetotelluric (AMT) and seismic refraction data from a test site. We inverted the near-surface field data to test the consistency of the recently proposed hypothesis on subsurface ‘lithofacies’ or structural classification based on resistivity-velocity interrelationships from joint inversion models. The MT-seismic relationship is found to be in excellent accord with that derived previously for dc resistivity and seismic data set at this test site. We suggest that joint MT-seismic structural classification is feasible and discuss the implications for deep imaging studies.

**Keywords:** Joint cross-gradients inversion, magnetotellurics, seismic refraction, lithofacies and structural classification

---

### INTRODUCTION

Collocated magnetotelluric (MT) and seismic refraction profiling are becoming increasingly popular in studies of the near-surface down to mantle depths [e.g. Meju et al., 2003; Gallardo & Meju, 2003,2006]. However, the field data are more commonly inverted separately resulting in MT resistivity and seismic velocity models that are structurally different for coincident survey lines and this has somewhat hindered the development of an objective and generic method for lithological or structural classification based on MT and seismic models, such as originally proposed for near-surface dc resistivity and seismic refraction studies [see e.g. Gallardo and Meju 2003, Fig.5].

The use of appropriately coupled joint inversion of MT impedance (apparent resistivity and phase) and seismic travel-time data from collocated experiments will result in better characterisation of heterogeneity and lead to improved understanding of the resistivity-velocity interrelationships in complex subsurface materials [Meju et al., 2003], necessary for lithological or structural classification [Gallardo and Meju, 2003,2006]. We have recently developed a cross-gradients MT-seismic inversion algorithm that can also handle any reliable a priori information that is available especially regarding the existence of smooth or sharp

structural boundaries [Gallardo and Meju 2006]. Our synthetic pilot studies of 2D MT and seismic refraction joint inversion have shown that coupled data inversion incorporating the cross-products of the resistivity and seismic velocity gradients as constraints, provides an effective structural linkage between the velocity and resistivity models [Gallardo and Meju, 2006]. It also leads to more accurate models and improves the structural conformity between the resistivity and velocity images without forcing or assuming the form of the relationship between them [Gallardo and Meju 2003,2004; Gallardo et al.,2005]. Our goal in this paper is to determine the 2D MT resistivity and seismic velocity interrelationship [Meju et al., 2003] at a field site used by Gallardo and Meju [2003] to develop their concept of ‘lithofacies’ classification based on joint inversion of near-surface dc resistivity and seismic data. We will evaluate the utility of the resulting models for lithological and/or structural classification. The significance of developing an objective lithofacies-structural classification based on joint 2D MT-seismic inversion derives from the wide range of probing depths potentially covered by both methods. This will facilitate the deduction of structural and lithological patterns from near-surface to mantle depths, necessary for understanding fundamental geological processes occurring in the Earth’s crust and mantle.

## JOINT INVERSION AND IMPLICATIONS

### The field measurements

We selected the AMT and seismic refraction data from the Quorn field site [Meju et al. 2003] studied by Gallardo and Meju [2003]. This site is characterized by a highly fractured granodioritic basement and heterogeneous sedimentary cover consisting of mudstone and glacial till. The seismic survey employed 2 m geophone spacing and four shot points along a 165 m transect that is orthogonal to the known local geological strike. The AMT data of interest in this study were recorded using 15 m long electric dipoles aligned in the seismic profiling direction and a magnetic induction coil placed in the orthogonal direction with a 15 m station interval. A total of 13 AMT stations were recorded over the frequency range 80 KHz to 1 Hz over a distance of 195 m on the seismic line. These AMT data correspond to the TM mode measurements. The apparent resistivity data show errors ranging from 1 to 10 percent and are deemed acceptable but the phase information was much noisier and hence have not been emphasized in the present study. All the AMT apparent resistivity data were corrected for static shift using coincident transient electromagnetic soundings [see Meju et al. 2003, Fig.2].

### Joint inversion of AMT and seismic first-arrivals

Each AMT datum was assigned the corresponding observational error from the actual field survey but the seismic data were assigned a standard deviation of 1ms. The subsurface model was discretized into rectangular cells exactly coincident to those used in Gallardo and Meju [2003] to permit a direct comparison. Unlike the joint DC-seismic inversion in Gallardo and Meju [2003,2004] that involved only smooth initial models, we started the AMT-seismic inversion process with layered models with velocity and resistivity increasing monotonically with depth. This will reduce the number of steps required in the iterative process as well as test the robustness of the algorithm. The joint inversion process was allowed initial target normalized misfits ( $\beta$ ) of 10 and gradually reduced to 1 as recommended in Gallardo and Meju [2004]. The smoothing factors were selected after some experimentation and we found that stable results were obtained using  $\alpha_{MT}=a_S=100$ . The final models obtained for a target normalized misfit of 1 are shown in **Figure 1**. The models obtained matched the seismic data well (to normalized rms misfit of 0.97) but less satisfactorily for the MT data which have a misfit greater than 1. The distributions of the normalized residuals for seismic and AMT data are presented in **Figure 2**. The images recovered show geometrical similarity as required by the cross-gradients constraint. These models show some refinements when compared to the results of separate AMT and seismic inversion given in Meju et al. [2003]. The differences can be quantified by

computing the cross-gradients values for the separate inversion models (**Figure 3a**) and joint inversion models (**Figure 3b**).

### Implications for lithofacies-structural classification

In **Figure 4** is shown the AMT resistivity and seismic velocity interrelationships as deduced from the joint inversion models (**Figure 1**). **Note** the distinct trends and the excellent agreement with those previously determined by *Gallardo and Meju* [2003] based on joint dc resistivity-seismic inversion. In **Figure 4**, the resistivity-velocity trend (numbered as trend 3) is associated with the deepest structural features. The AMT-seismic joint inversion results thus not only confirm the existence of such trends but also demonstrate the structural consistency that can be achieved and the resistivity-velocity interrelationships to be expected from joint inversion of AMT and seismic refraction data. It can be expected that the same deductions would apply to models from deep regional MT and seismic surveys.

## CONCLUSION

We have successfully applied a 2D cross-gradients inversion technique to MT and seismic travel-time field data from the Quorn test site where comparative data are available, and obtained results that are in excellent agreement with those obtained independently from joint 2D inversion of collocated dc resistivity and seismic data. The joint inversion models recovered consistent structural features of the subsurface. We suggest that joint inversion of collocated MT-seismic profiles and the use of the results in structural or lithological classification will lead to improved subsurface characterization in complicated geological terrains and should be seen as the way forward in subsurface studies. We plan to extend this inversion method to the joint analysis of MT and wide angle reflection data.

## REFERENCES

- Gallardo, L. A., and M. A. Meju, 2003, Characterization of heterogeneous near-surface materials by joint 2D inversion of dc resistivity and seismic data, *Geophys. Res. Lett.*, 30(13), 1658, doi:10.1029/2003GL017370.
- Gallardo, L. A., and M. A. Meju, 2004, Joint two-dimensional DC resistivity and seismic travel time inversion with cross-gradients constraints, *J. Geophys. Res.*, 109, B03311, doi:10.1029/2003JB002716.
- Gallardo, L.A., Meju, M.A. and Flores-Perez, M.A., 2005. A quadratic programming approach for joint image reconstruction: Mathematical and geophysical examples. *Inverse Problems* 21, 435-452.

Gallardo, L.A. and Meju, M.A., 2006, Joint 2D cross-gradients imaging of magnetotelluric and seismic travel-time data for structural and lithological classification. *Geophys. J. Int.* (in review).

and seismic velocity in heterogeneous near-surface materials. *Geophys. Res. Letts.*, 30, (7), 1373-1376.

Meju, M.A., Gallardo, L.A., and Mohamed, A.K., 2003, Evidence for correlation of electrical resistivity

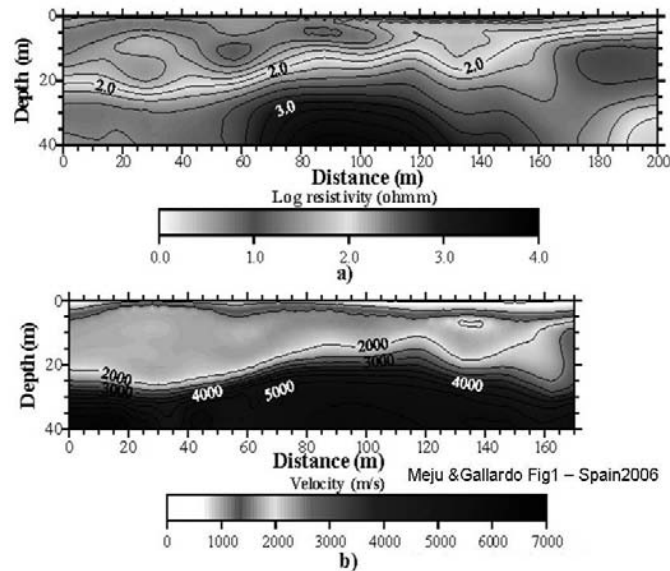


Figure 1. a) AMT resistivity model and b) seismic velocity model for the Quorn profile data obtained by joint inversion of AMT apparent resistivity and seismic traveltimes (Gallardo & Meju,2006). The inverted triangles denote the sounding positions and the arrows the position of the seismic sources

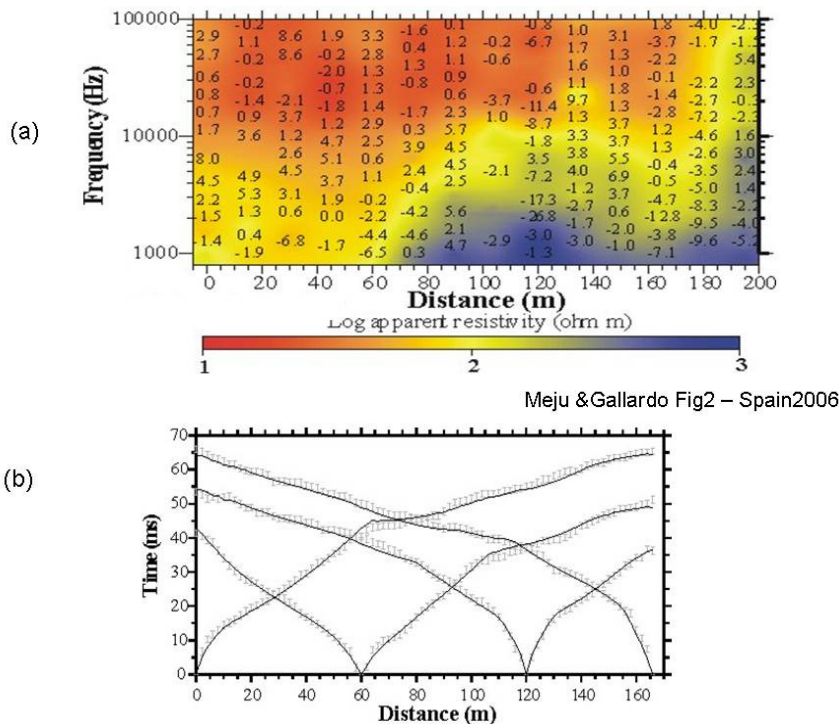


Figure 2. a) Image of the measured AMT apparent resistivity data used for joint inversion. The annotated values correspond to selected normalized residuals achieved after the Joint Inversion process plotted in their corresponding position. b) Observed travel time data (Grey bars) and travel times computed using the model of Figure 6b (Solid lines). The actual bars show the standard deviation of the data.

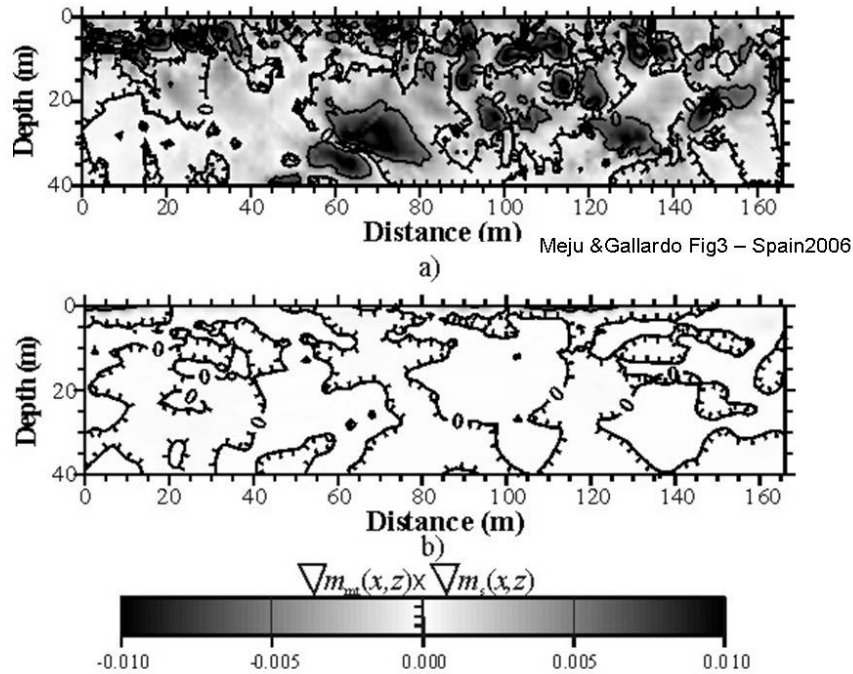


Figure 3. Cross- gradients values computed from the MT and seismic models for Quorn profile. a) using models obtained from separate inversion. b) using the models obtained from joint inversion of the same data sets.

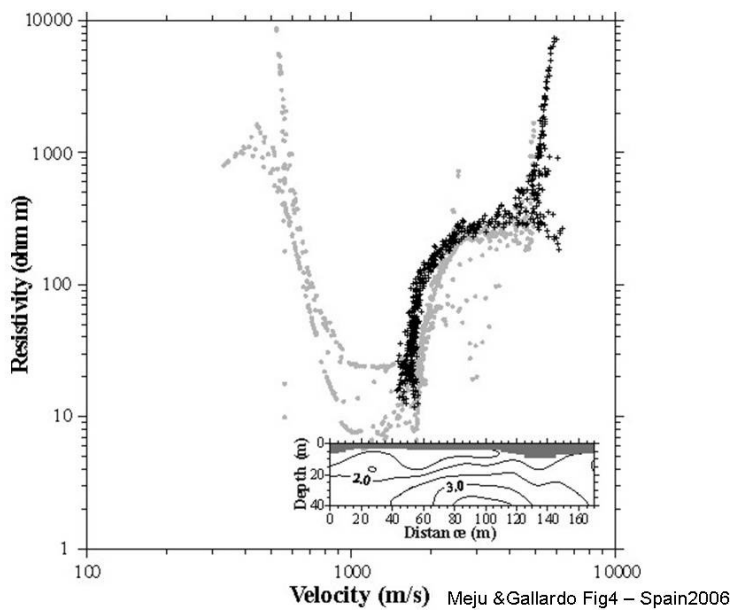


Figure 4. Comparison of resistivity and seismic velocity cross-plots for the Quorn profile. The grey dots correspond to those from dc-seismic joint inversion [Gallardo and Meju, 2003]. The black crosses are from the AMT-seismic joint inversion results. The inset shows the actual distribution of the model cells (pixels) corresponding to the plotted trend overlying the AMT resistivity image. Note the coincidence of the AMT and dc trends for velocities greater than 1500 m/s.

## S4-E5

*IGAGA WG 1.2 on Electromagnetic Induction in the Earth  
Extended Abstract 18<sup>th</sup> Workshop  
El Vendrell, Spain, September 17-23, 2006*

---

### **Joint inversion of MT and seismic receiver function data using a genetic algorithm**

Max Moorkamp, Dublin Institute for Advanced Studies, Dublin, Ireland  
Alan G. Jones, Dublin Institute for Advanced Studies, Dublin, Ireland  
C.K Rao, Dublin Institute for Advanced Studies, Dublin, Ireland

---

#### **SUMMARY**

We use a genetic algorithm to jointly invert magnetotelluric and seismic receiver function data. Genetic algorithms have become popular in multi-objective inversion for several reasons: They are suited for highly non-linear problems, they do not require weighting of the individual datasets and they can produce the trade-off between fitting the datasets within the inversion. An important aspect in joint inversion of data that is influenced by different physical quantities is to distinguish cases where the data are due to correlated structures in the subsurface from cases where they are not. We create a suite of synthetic test problems to see how the genetic algorithm can help to distinguish between these cases. The results suggest that it is possible in principle, but requires a considerable amount of computing power except in simple cases. These results are encouraging and motivate us to tackle the inversion of real data. We invert data from one station in central Ireland. The inversion achieves a good data fit for both datasets, but the question of compatibility remains inconclusive.

**Keywords:** magnetotellurics, receiver functions, joint inversion, genetic algorithms

---

#### **INTRODUCTION**

Creating models of the Earth from measured data is an essential part of any geophysical survey. Depending on the type of measured data, different limitations on resolvable physical quantities and spatial resolution exist. In addition, limited and noisy data makes the mapping between models and data non-unique. One possibility to improve the situation is to combine several datasets in the inversion. If all the datasets are sensitive to the same physical properties, this process is conceptually straightforward and one can expect the resulting model to be at least of the same quality as the individual models or better.

The situation changes if datasets are combined that react to different physical properties, such as electromagnetic and seismic data. On the one hand one can hope to obtain more information about the subsurface, reduce the number of acceptable models and dampen the influence of noise, on the other hand this approach can fail completely if the datasets are independent, i.e., influenced by different structures. Evaluating and critically examining the inversion results then becomes even more important than in traditional inversion of single datasets.

Ideally the inversion scheme itself provides a measure in how far the datasets are compatible. Usually the RMS-misfit is used to quantify the quality of the model, a low misfit indicating a model that represents the data well. With several datasets this measure of quality becomes problematic. If the misfit is very high for one or more datasets, the model can certainly be rejected as unreliable. In the presence of moderate noise and medium misfit for all datasets, the question arises whether the differences between observed and predicted data are a result of the noise, limitations in the forward modelling or a violation of the underlying assumption that both datasets are influenced by the same structures. It is therefore necessary to use other information to evaluate the inversion model.

#### **GENETIC ALGORITHMS IN JOINT INVERSION**

Genetic algorithms are a class of stochastic optimization algorithms that use techniques analogous to biological evolution. They have been successfully used in a number of non-linear optimization tasks including inversion of geophysical data (Everett and Schultz, 1993; Schwarzbach et al., 2005). In recent years they have gained particular importance in the

field of multi-objective optimization. This is due to two beneficial properties: First, a weighting of the datasets is not required, and second the inversion does not yield a single output model but produces the trade-off between fitting the different datasets.

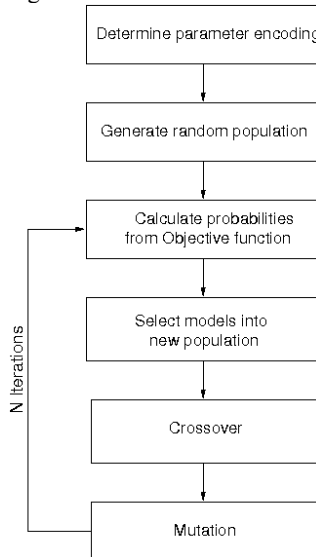


**Figure 1** Program flow of genetic algorithm inversion

Schwarzbach et al. (2005) have used the popular algorithm NSGA-II (Deb, 2002) to produce the L-curve, the trade-off between misfit and model roughness, for geoelectric data. The general setup for any type of genetic algorithm is shown in figure 1. The details for each of the individual steps vary and can be adjusted to the particular problem, but the overall structure remains identical for all types of genetic algorithms.

Another advantage of genetic algorithms is that they have been developed for highly non-linear problems. Sambridge et al. (2006) recently showed that the problem of receiver function inversion can be multi-modal. Any gradient-based approach with a starting model that is not sufficiently close to the true model will likely converge to a false minimum. With a genetic algorithm there is a chance that the algorithm will escape the false minimum, but as it is a stochastic method there is no guarantee that it does. Repeated runs of the genetic algorithm can avoid this problem. This is, of course, also possible with a gradient-based approach in which the starting model is changed in several runs. The disadvantage then is that it requires much more user interaction and it is not clear in how far the starting model has to be perturbed to account for the complexity of the misfit surface.

We use our own implementation of NSGA-II (Deb, 2002) to jointly invert magnetotelluric and receiver

function data. The inversion also allows us to include regularization and thus includes three possibly competing criteria that have to be minimized simultaneously. Under these circumstances determining optimum weights for each criterion would be impossible *a priori*. The genetic algorithm solves this problem by not requiring the user to weight the data and implicitly determining these weights. Also we will use the trade-off between the fits to assess the compatibility of the two datasets.

## THE DATA

For this study we jointly invert receiver function and magnetotelluric data. Receiver functions are transfer functions calculated from 3 component recordings of teleseismic events. Most commonly used is the transfer function between the radial and vertical component in a window around the P-wave arrival. This transfer function highlights wave conversions at interfaces in the crust and mantle below the recording site and does not depend on far structures along the ray path. These properties make it possible to create localized models and a common procedure is to perform 1D inversion for each site separately.

The sensitivity to crustal and mantle structures without the need of a global teleseismic model make receiver functions ideal to test the hypothesis of correlation between electric and seismic structure on a lithospheric scale. Also a study of MT and receiver function data in Canada suggests that electrical and seismic structures can be correlated (Jones et al., 2002).

In early 2004 we installed 22 magnetotelluric sites collocated with previously installed seismic stations in central Ireland. This provides the opportunity for a detailed comparison of seismic and MT data. At each site Phoenix V5-2000 and long-period LIMS systems recorded for 2 days and 2-4 weeks, respectively. Unfortunately the frequency band between 300 Hz and 1 Hz was corrupted by strong electric fence signals but the long period signal between 1 s and 10,000 s was generally good quality. At most sites the penetration depth is 100 km or deeper, covering the whole lithosphere in this area.

## SYNTHETIC TESTS

To assess the capabilities of the algorithm, and define criteria that allow a distinction between correlated and uncorrelated seismic and electric structure, we have studied a number of synthetic test cases. We will show three realistic examples that highlight the possibilities and limitations. We did not include regularization in these examples, as it would require 3 dimensional plots that would obscure the main points of this study. The

exclusion of regularization has two effects: First the obtained inversion models can exhibit unrealistic fluctuations of parameters in adjacent layers, and second the misfit of the inversion results will be lower than with regularization.

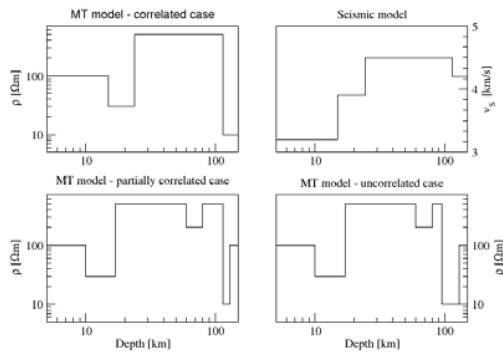


**Figure 2** MT and seismic models used to generate the input data for the synthetic test cases.

The three cases we consider for our synthetic study are:

1. Electric and seismic structure correlate perfectly, i.e. changes in seismic velocity are accompanied by a change in electrical conductivity and vice versa,
2. There is no correlation within the crust, but the lithosphere-asthenosphere boundary correlates and
3. No correlation between the two at all.

For the seismic data the PREM model, with a stronger lithosphere asthenosphere velocity contrast, is used to calculate the input data. The models to generate the magnetotelluric input data are perturbed for each test scenario to reflect the different correlations. Figure 2 shows an overview of the seismic and MT models used to generate the input data for the test scenarios.

We run the genetic algorithm with a population size of 1000 for 100 iterations. This corresponds to 100,000 forward modellings. In the 1D case each forward modelling is computationally cheap, but for higher dimensions this would either require access to a cluster or result in long run times. The resulting set of models for each scenario is displayed in figure 3. Plotting MT-misfit against receiver function misfit allows assessment of the trade-off between fitting the two datasets. For the perfectly correlated case the result is similar to the L-curve in regularization. The bend of the L is very pronounced, which makes it easy to select the preferred model. The model right at the bend fits both datasets equally well. Any deviation from this model might improve the fit of one dataset slightly but at the cost of a much higher deterioration in the fit for the other dataset.

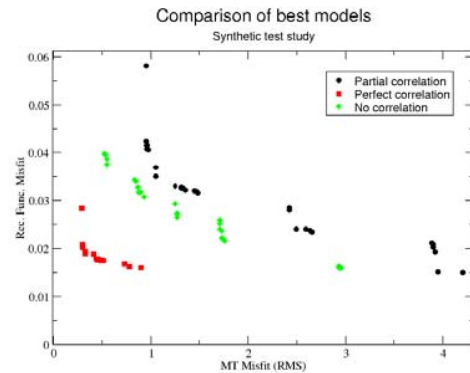


**Figure 3** Final range of models generated by the genetic algorithm for the three synthetic test cases.

For the other two cases the situation is less simple. Both of them show a consistently larger misfit than the perfectly correlated case, but surprisingly the uncorrelated case achieves a lower misfit for both datasets than the partially correlated case. This behaviour reflects the stochastic nature of the algorithm. Especially in later iterations small improvements in misfit often need a lot of forward calculations and the algorithm might terminate too early. A criterion that distinguishes the three scenarios better than the achieved misfit is the shape of the trade-off curve. In contrast to the single L for the correlated case, the two curves consist of several L-shaped clusters that are separated by gaps. Also the overall shape is more close to a straight line, than an L.

This behaviour can be explained as follows: Models that achieve a low MT-misfit (in figure 3 on the upper left) have a similar structure to the MT input model. Consequently the receiver function misfit is high when the input models are very different. Small variations of this model result in slightly improved fits of either the receiver function or the MT data reflected by the cluster of points. When the deviations become too large the algorithm finds another misfit minimum. This process repeats until finally the model matches the seismic model (lower right corner). The receiver function misfit is now low, but the MT misfit high. The existence of several clusters reflects the multi-modality of the misfit surface. The models associated with these clusters reflect either the MT data, the receiver function data or a mixture of aspects of both.

One limitation of this criterion is that it does not reveal where the seismic and electric structures disagree. The misfit is a global quantity that depends on all data points. An inspection of the output models helps to identify common features and differences.

### APPLICATION TO DATA

We apply the genetic algorithm to data from the ISLE-MT experiment. This inversion is only preliminary as the receiver function data is from a single event, usually several receiver functions from different events are stacked together to reduce the influence of noise. To minimize the influence of higher dimensionality for the MT data, we invert for the Berdichevsky invariant  $0.5 (Z_{xz} - Z_{zx})$  (Berdichevsky, 1976).

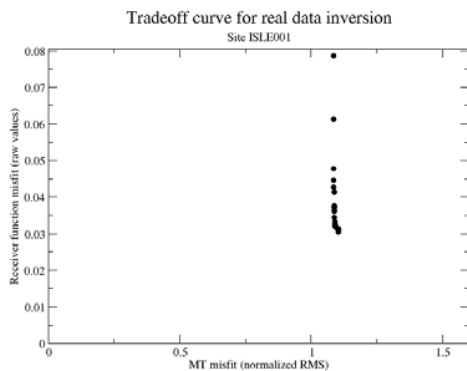


**Figure 4** Tradeoff between MT and receiver function misfit for a real data example.

We achieve a low misfit for both receiver function and MT data for a number of models. The tradeoff curve for MT misfit and receiver function misfit (figure 4) shows very little variation in MT misfit, but large variations for the receiver function misfit. This suggests that the datasets are compatible. There are only a limited number of models that achieve an acceptable receiver function fit. As mentioned above this is the very first inversion of real data and much more work and analysis will be carried out before the results can be interpreted in terms of geological implications.

### CONCLUSIONS

The application of a genetic algorithm for joint inversion of magnetotelluric and receiver function data has been successful. In addition to fitting both datasets

when the structures are correlated we can use the trade-off between fitting the different datasets to distinguish between correlated and uncorrelated cases. Further work is needed to examine whether this conclusion is robust in the presence of different types of noise.

### ACKNOWLEDGEMENTS

We thank M. Adlem, A. Avdeeva, D. Byrne, M. Hamilton and J. Spratt for help with installing the MT sites.

This project is funded by IRCSET basic research grant SC/2003/237.

### REFERENCES

- Berdichevsky, M.N. and Dmitriev, V.I., 1976, Basic principles of interpretation of magnetotelluric sounding curves, in Adam A., Ed., *Geoelectric and geothermal studies: Budapest, Akademiai Kiado*, 165-221
- Deb, K., Pratap, A., Agarwal, S. and Meyarivan, T., 2002, A Fast and Elitist Multiobjective Genetic Algorithm: NSGA-II, *IEEE Transactions on evolutionary computation*, 6, 2, 182-197
- Everett, M. E. and Schultz, A., Two-dimensional nonlinear magnetotelluric inversion using a genetic algorithm. *J. Geomag. Geoelectr.*, 45, 1013-1026, 1993
- Jones, A.G, Snyder, D., Hammer, S., Asudeh, I., White, D., Eaton, D. and Clarke, G., 2002. Magnetotelluric and teleseismic study across the Snowbird Tectonic Zone, Canadian Shield: A neoproterozoic mantle suture?, *GRL*, 29,17,1829
- Sambridge M, Beghein, C., Simons, F. and Snieder, R. 2006. How do we understand and visualize uncertainty?, *The Leading Edge*, 25, 543-546
- Schwarzbach, C., Boerner, R.-U. and Spitzer, K., 2005. Two-dimensional inversion of direct current resistivity data using a parallel, multi-objective genetic algorithm, *GJI*, 162, 685-695

## **Application of ANN techniques to combined analysis of magnetotelluric and other geophysical data in the northern Tien Shan crustal area**

V. Spichak<sup>1</sup>, A. Rybin<sup>2</sup>, V. Batalev<sup>2</sup>, Y. Sizov<sup>1</sup>, O. Zakharova<sup>1</sup>, and A. Goidina<sup>1</sup>

<sup>1</sup>Geoelectromagnetic Research Centre IPE RAS, Lab EM data interpretation methodology, Troitsk, Russia

<sup>2</sup>Scientific Station IVTRAN RAS, Bishkek, Kyrgyzstan

---

### **SUMMARY**

The paper discusses the application of the artificial neural network (ANN) techniques to combined analysis of MT and other geophysical data. Use of the ANN technique (backpropagation scheme) enabled to get the preliminary 3D resistivity model of the northern Tien Shan seismic area. The most remarkable features of this model are: presence of the deep diagonal fault crossing the studied area from South-East to North-West and general decreasing of the resistivity in the same direction.

The maximal correlation similitude (MCS) technique enabled to reveal the areas in the northern Tien Shan upper crust, where the correlation of the bulk resistivity with EQ hypocenters' density is maximal. The spatial distribution of these zones indicate that EQ hypocenters concentrate either in very resistive (firm and brittle) areas of the crust or in the vicinity of the deep faults crossing the area.

It was found that the temperature well records and the conductivity data manifest rather good correlation. The maximal correlation ratio determined by MCS technique is equal to 0.95 and is achieved over the set of 45 temperature records selected from the wells Chaldovar-2P, Belovodskii-2P, Fos-1, Alamedin-907 and Alamedin-917. The preliminary analysis of this result indicates that selected locations are characterized by simultaneous increase of both the temperature and conductivity with depth. This property could be, probably, considered as one of the necessary conditions for local homogeneity of the geological medium and used as a constrain for reconstruction of the geological model from the resistivity one.

**Keywords:** Artificial neural networks, correlation analysis

---

### **INTRODUCTION**

The artificial neural networks are used nowadays in various geophysical applications. They are known as flexible mathematical tools capable of efficient data processing, analysis and inversion (Raiche, 1991; Poulton, 2001). Methodological findings published in (Spichak and Popova, 2000) formed a good basement for subsequent ANN applications aimed at detection of 3D fault macro-parameters from CSAMT data (Spichak et al., 2002) and 3D MT tomography of volcanoes (Spichak et al., 2004, 2006).

This paper is aimed, first, at reconstruction of 3D resistivity model of the northern Tien Shan seismic area from MT data and, second, at estimation of the correlation between its resistivity distribution, on the one hand, and data on seismicity and temperature available from well logs.

### **3D RESISTIVITY IMAGE OF THE STUDIED AREA**

In the Bishkek geodynamical test site complex geophysical studies were performed aimed at estimation of seismic activity of the region and its manifestations in geophysical fields measured on the ground. With this purpose, a magnetotelluric sounding of the region was carried out, and its results were compared with the measurements of seismic velocities and borehole temperatures as well as with spatial distribution of the hypocenters of seismic activity.

Magnetotelluric data collection was arranged in 7 profiles crossing two major E-W trending faults, which bound the Kyrgyz Range to the foreland Chu Basin (Figure 1). The data were measured in 59 locations at 47 periods ranging from 0.06 s to 1585 s and covered the area bounded by latitudes 42.5 and 43.0 (°N) and longitudes 73.5 and 75.1 (°E).

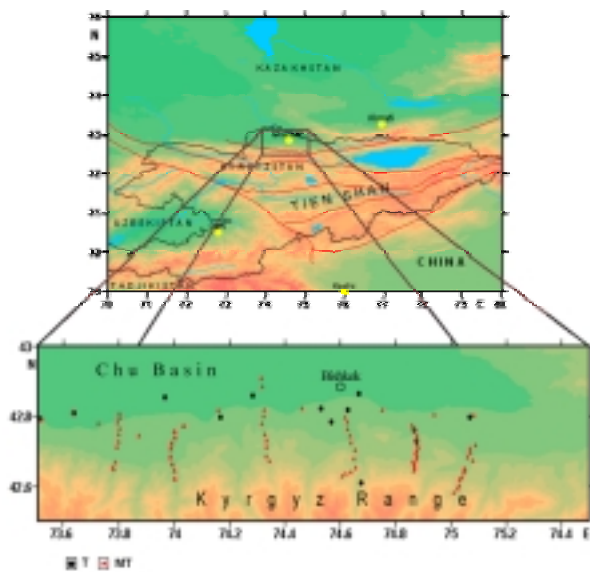


Figure 1. Map of the site locations.

### Backpropagation technique

In estimating the resistivity distribution in the northern Tien Shan area we used one of the 'learning-with-a-teacher methods', i.e., the error back-propagation (BP) technique. In such an approach there are two stages in the inversion procedure: training of the network and its testing, or recognition (the inversion itself). In the learning (or training) stage, the 'teacher' specifies the correspondence between chosen input and output data. The system could be considered as an  $n$ -layer network in which every neuron of a given layer is somehow connected with the neurons of other layers. A signal comes to the input layer of neurons from outside the system, but its magnitude at the neurons of the other layers depends on the signal magnitudes and connection weights of all associated neurons of the previous layer. Moreover, the net response of an artificial neuron is described by a non-linear function.

The ANN architecture in our studies was as follows: an input layer that had three neurons (two geographical coordinates of MT sites plus apparent depth); two hidden layers with 20 and 15 neurons, and an output layer that had one neuron, corresponding to the resistivity to be estimated. The learning rate ( $\alpha$ ) was equal to 0.01 and the momentum ( $\beta$ ) equal to 0.9. The neural network was taught until it reached a threshold accuracy of 1%, which, according to experience ce with the neural network (Spichak and Popova, 2000), was sufficient to achieve 5 to 10% accuracy in the recognition of the target parameters.

### ANN inversion of MT data

The data analysis was carried out using 1D Occam's inversion of the apparent resistivity determinant. Further, in order to get the idea about 3D resistivity distribution in the studied area the artificial neural network inversion was carried out.

After teaching the ANN was used in order to reconstruct the resistivity structure in the studied area. The preliminary 3D model is very resistive in the South-East part and becomes more conductive in the North-West direction (Figure 2). In particular, a very conductive zone with the resistivity less than 10 Ohm.m is detected at the depths 3-5 km around the location of the temperature well Chaldovar-2P (red spot in the North-West corner of the Figure 2a) that correlates with low seismic velocity ( $V_p$ ) zone in the upper 5 km (Adamova and Sabitova, 2004).

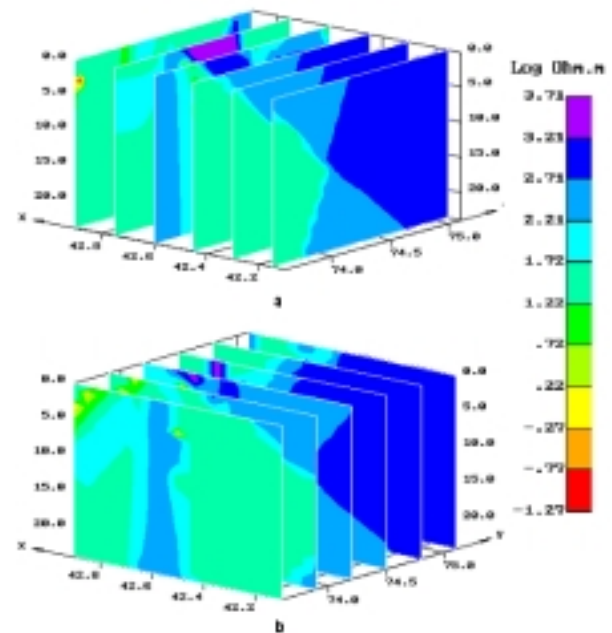


Figure 2. Resistivity model of the northern Tien Shan crustal area: a –slices in latitudinal direction; b – slices in longitudinal direction.

Another remarkable feature of the constructed model is the presence of the deep diagonal fault crossing the studied area from South-East to North-West.

### CORRELATION OF THE RESISTIVITY AND SEISMICITY

ANN taught by the MT data was used further in order to estimate the correlation between the resistivity distribution, on the one hand, and the seismic velocity, on the other hand. To this end the resistivity values were forecasted in the locations of the two longitudinal

and two latitudinal profiles, where the P and S wave velocities were measured earlier (Ghose et al., 1998). The results of the ANN analysis indicate a good correlation between the resistivity and P wave velocity distributions along two profiles crossing the faults.

A correlation between the bulk resistivity and the density of the earthquake hypocenters detected in this area was estimated using the maximal correlation similitude (MCS) method proposed in (Spichak et al., 2006) for combined analysis of different geophysical data. This method is also useful in the case when one has to fill the gaps in the data by using the data of another type that provides maximal correlation ratio with the former one.

### Maximal correlation similitude method

The idea of the method is as follows. Let a multitude  $E = \{\mathbf{x}\}$  be given consisting of  $n$  pairs  $\mathbf{x} = (x_1, x_2)$  of the values of two, generally speaking, random quantities. Selective correlation coefficient of these quantities equals

$$r_E = \frac{n \sum_{\mathbf{x} \in E} x_1 x_2 - \left( \sum_{\mathbf{x} \in E} x_1 \right) \left( \sum_{\mathbf{x} \in E} x_2 \right)}{\sqrt{n \sum_{\mathbf{x} \in E} x_1^2 - \left( \sum_{\mathbf{x} \in E} x_1 \right)^2} \sqrt{n \sum_{\mathbf{x} \in E} x_2^2 - \left( \sum_{\mathbf{x} \in E} x_2 \right)^2}} \quad (1)$$

Then such a subset  $A \subseteq E$  consisting of  $m \leq n$  pairs that provides a maximal "partial" correlation coefficient

$$r_A = \frac{m \sum_{\mathbf{x} \in A} x_1 x_2 - \left( \sum_{\mathbf{x} \in A} x_1 \right) \left( \sum_{\mathbf{x} \in A} x_2 \right)}{\sqrt{m \sum_{\mathbf{x} \in A} x_1^2 - \left( \sum_{\mathbf{x} \in A} x_1 \right)^2} \sqrt{m \sum_{\mathbf{x} \in A} x_2^2 - \left( \sum_{\mathbf{x} \in A} x_2 \right)^2}} \Rightarrow \max \quad (2)$$

is sought by means of the neural network mathematics.

Since this mathematical problem, evidently, has a non-unique solution, the desired subset is found by posing a natural requirement of one-to-one correspondence between the values of two functions.

### Correlation between the bulk resistivity and density of EQ hypocenters

By means of MCS technique 57 elementary domains surrounding the hypocenters' locations are selected that provide the correlation coefficient between the bulk resistivity and EQ hypocenters equal to 0.79 (Figure 3).

It is seen from the Figure 3 that EQ hypocenters concentrate either in very resistive (firm and brittle) areas of the upper crust or in the vicinity of the deep faults crossing the area.

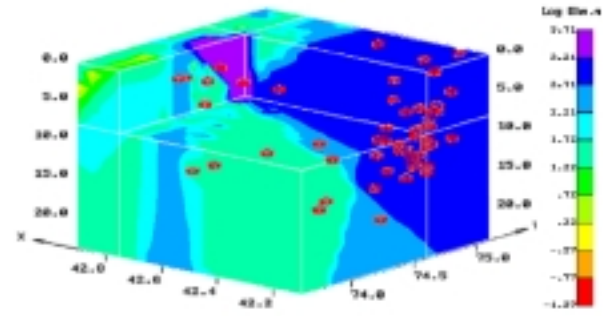


Figure 3. Volume resistivity model of the northern Tien Shan crustal area. Maximal correlation zones are marked by red color.

### CORRELATION OF THE CONDUCTIVITY AND TEMPERATURE DISTRIBUTIONS

The correlation between the conductivity distribution revealed by ANN and temperature well logs (Figure 1) was estimated. The analysis of the results enables one to make the following conclusions:

- correlation coefficients are independent on the spacing between the well and the nearest MT site;
- the worst values of correlation coefficients are due to the specificity of geological structure of the studied area between the well and MT site: in some cases this is the presence of tectonic dislocations (faults); in other cases this is local inhomogeneities that affect the behavior of electric conductivity and, lastly, this is the presence of lateral low-temperature flows;
- a number of temperature/conductivity profiles manifest rather good correlation.

In order to find the subsets of the temperature records, on the one hand, and corresponding conductivity values, on the other hand, which provide the maximal correlation ratio we have used the MCS method mentioned above. It was determined that the best correlation (ratio being equal to 0.95) is achieved at 45 temperature locations in the wells Chaldovar-2P, Belovodskii-2P, Fos-1, Alamedin-907 and 917.

The preliminary analysis of this result indicates that selected elementary domains are characterized by simultaneous increase of both the temperature and conductivity (Figure 4 shows the graphs of the conductivity and temperature versus depth in the well Chaldovar-2P (a) and adjacent MT site (b)), which could be, probably, used as a necessary condition for local geological homogeneity.

### CONCLUSIONS

Application of the artificial neural network technique enabled to get the preliminary 3D resistivity model of the northern Tien Shan seismic area. The most remarkable features of this model are: presence of the

deep diagonal fault crossing the studied area from South-East to North-West and general decreasing of the resistivity in the same direction.

Using the maximal correlation similitude (MCS) technique enabled to reveal the areas in the northern Tian Shan upper crust, where the correlation of the bulk resistivity with EQ hypocenters' density is maximal. The spatial distribution of these zones indicate quite clearly that EQ hypocenters concentrate either in very resistive (firm and brittle) areas of the crust or in the vicinity of the deep faults crossing the area.

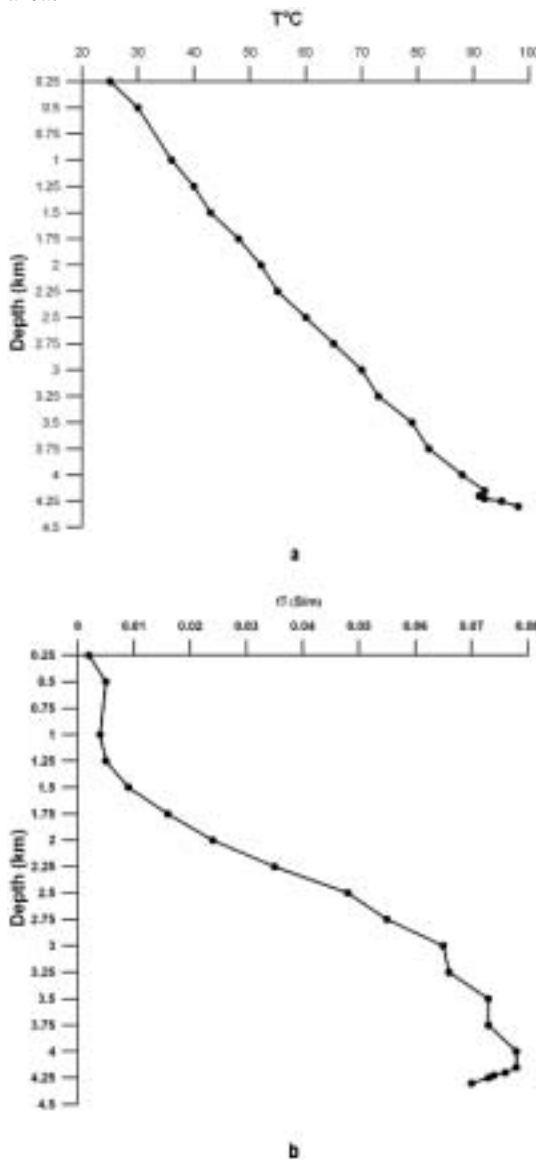


**Figure 4.** Temperature (a) and conductivity (b) versus depth graphs in the Chaldovar-2P well and adjacent MT site.

It was found that the temperature and conductivity data manifest rather good correlation. The maximal

correlation zones determined by MCS technique provide the ratio equal to 0.95. The preliminary analysis of this result indicates that selected domains are characterized by simultaneous increase of both the temperature and conductivity with depth. This property could be, probably, considered as one of the necessary conditions of local homogeneity of the geological medium. Its application to joint analysis of MT and geothermic data may lead to more correct projection of the resistivity model to the geological one.

#### ACKNOWLEDGEMENTS

The study was supported by INTAS (grant 03-51-3327) and RFBR (grants 04-05-65103 and 05-05-85013).

#### REFERENCES

- Adamova, A.A., and Sabitova, T.M., 2004. 3D seismic velocity model of the Tien Shan crust revealed by seismic tomography. *Izv. Fizika Zemli*, 5, 58-68.
- Ghose, S., Hamburger, M., and Virieux J., 1998. Three-dimensional velocity structure and earthquake locations beneath the northern Tien Shan of Kyrgyzstan, Central Asia. *J. Geophys. Res.*, 103, B2, 2725-2748.
- Poulton, M. (ed.), 2001. *Computational neural networks for geophysical data processing*. Pergamon, Amsterdam, 335pp.
- Raiche, A., 1991. A Pattern Recognition Approach to Geophysical Inversion Using Neural Networks. *J. Geophys. J. Int.*, 105, 629 - 648.
- Spichak, V.V., Borisova, V.P., Fainberg, E.B., Khalezov, A.A., Goidina, A.G., 2006. Electromagnetic tomography of the Elbrus volcanic center by magnetotelluric and satellite data. *Vulkanologiya i seismologiya* (in Russian) (in press).
- Spichak, V.V., Fukuoka, K., Kobayashi, T., Mogi, T., Popova, I., and Shima, H., 2002. Artificial neural network reconstruction of geoelectrical parameters of the Minou fault zone by scalar CSAMT data. *J. Appl. Geoph.*, 49 (1/2), 75-90.
- Spichak, V.V., and Popova, I.V., 2000. Artificial neural network inversion of MT - data in terms of 3D earth macro - parameters. *Geoph. J. Int.*, 42, 15-26.
- Spichak, V.V., Yamaya, Y., and Mogi, T., 2004. ANN modeling of 3D conductivity structure of the Komagatake volcano (Hokkaido, Japan) by MT data. *Proc. IV Int. Symp. MEEMSV-2004, La Londe Les Maures, France*, 121-122.

## S4-E7

### **Interpretation of detailed and semi-detailed magnetotelluric data constrained by geological and seismic data; examples from Polish Outer Carpathians**

**Michał STEFANIUK, AGH University of Science and Technology, Krakow, Poland**

**Marek WOJDYŁA, Geophysical Exploration Company, Warsaw, Poland**

#### **SUMMARY**

The study area is situated in the marginal zone of Polish Outer Carpathians in the extension zone of major structures of the Paleozoic platform, which occurs in front of the Carpathian overthrust. The main problems of geological investigations in the Polish Outer Carpathians include recognising of the structure and lithology differentiation of the flysch cover and subflysch basement. The Outer Carpathians are built of a thick complex of flysch sediments and have the form of an accretion prism. Intense tectonics of the flysch cover generates a complex spatial distribution of them and as a result a complex geophysical field pattern that is difficult to interpret (Stefaniuk et al. 2005). It was necessary to make integrated geophysical and geological data interpretation including seismic, gravimetry, well-logging and magnetotelluric methods. Magnetotelluric measurements were taken with the use of MT-1 system of Electromagnetic Instruments Incorporation (EMI), Richmond, California, USA. The time series of MT field components were recorded over a frequency range of 500 – 0.001 Hz. As it was mentioned before, a series of magnetotelluric soundings was made along one profile with a measurement step of 1500 m. To eliminate the effects of near-surface non-homogeneities, a short continuous profiling was made instead of a single sounding. The magnetotelluric continuous profiling was made along the second profile. The recorded time series were processed with the use of standard remote reference and robust data processing procedures. There were two stages of the quantitative interpretation. At the first stage, the analysis of so-called parametric soundings located near deep boreholes was made. At the second stage, 2D automatic inversion was applied.

**Keywords:** magnetotellurics, constrained inversion, integrated interpretation, flysch structure

---

## INTRODUCTION

The main problems of geological investigations in the Polish Outer Carpathians include recognising of the structure and lithology differentiation of the flysch cover and subflysch basement. The Outer Carpathians are built of a thick complex of flysch sediments and have the form of an accretion prism. The Carpathian overthrust is built of strongly folded, cut by tectonic zones flysch sediments in which dominate alternating silty-clayey and sandstone layers with varied thickness. The layers are characterized by strong differentiation of petrophysical parameters. Intense tectonics of the flysch cover generates a complex spatial distribution of them and as a result a complex geophysical field pattern that is difficult to interpret (Stefaniuk et al. 2005). It was necessary to make integrated geophysical and geological data interpretation including seismic, gravimetry, well-logging and magnetotelluric methods.

Geological formations building the flysch orogen and upper sedimentary part of the basement in the outer zone of the Carpathian overthrust are supposed to be hydrocarbon-prospective, so that they have been targets of geophysical and geological surveys (Gorecki et al. 2004). Numerous gas fields were discovered in Miocene complexes and their Mesozoic and Paleozoic sedimentary basement in the Carpathians' foreland and beneath the outermost part of the overthrust. A few small oil deposits were also found there. As a result, investigations were extended south where the prospective complexes rest beneath strongly folded flysch cover of the Carpathian overthrust. However interpretation of surface seismic data was difficult, mainly because of the specific complex geology of the Carpathian overthrust and its thickness increasing south. The above mentioned reasons caused that it was necessary to search for methods of recognition of the structure and lithology variations of the flysch cover as

well as supplement interpretation of reflection seismic data. To do this, the magnetotelluric method was applied.

A few semi-detailed and continuous MT profiles were designed in the marginal zone of the Carpathian overthrust to study the structure and lithology of the flysch cover and its basement. This paper presents interpretation of MT data from two profiles located southeast of the town of Rzeszów, within the marginal zone of the Carpathian overthrust. One profile was semi-detailed with a measurement step of 1500 m, while the other was continuous. The study area contained a few deep boreholes reaching the Carpathians basement; moreover, the refraction seismics survey was made along several profiles. This allowed the automatic inversion of MT data to be well constrained and interpretation results to be verified. The analysis of resistivity changes of the flysch series was based on well-logging data in relation to the stratigraphy, porosity and pore water salinity.

## OUTLINE OF GEOLOGY

The study area is situated in the marginal zone of Polish Outer Carpathians in the extension zone of major structures of the Paleozoic platform, which occurs in front of the Carpathian overthrust. The geology of the area is complex as a result of intense tectonics and erosional cuttings (Stefaniuk et al. 2005). Three main structural stages could be distinguished in the area:

- the Sub-Miocene basement consisting of Precambrian, Paleozoic and Mesozoic formations;
  - Miocene mollasses of the Carpathian foredeep;
-

- the Carpathian overthrust represented by Skole and Stebnik tectonic-and-stratigraphic units.

The oldest formation of the platform-type basement consists of metamorphic Precambrian rocks, partly overlain by a complex of clastic sediments of Lower Paleozoic. Above them, clastic and carbonate formations of Upper Paleozoic and Mesozoic occur. A strongly tectonically deformed complex of clastic Miocene sediments of different thickness that is overthrust by flysch structures consisting of geosynclinal Mesozoic and Cenozoic formations covers the platform-type basement.

The tectonics of the area was probably constituted during the latest phases of the Alpine orogenesis. The sub-Miocene basement is cut by two systems of normal faults with directions of strike NW-SE and SW-NE, and divided into several blocks. The tectonics of the autochthonous Miocene formations is conformable with the tectonics of the deeper basement. The thickness of this formation decreases to south to a thin layer, which remained on the Meso-Paleozoic erosion surface as a result of shearing by the thrusting-over Carpathians. The tectonic style of the flysch cover is completely different from the basement tectonics.

#### **TECHNICAL AND METHODOLOGICAL PROBLEMS OF SURVEYS**

Magnetotelluric measurements were taken with the use of MT-1 system of Electromagnetic Instruments Incorporation (EMI), Richmond, California, USA. The time series of MT field components were recorded over a frequency range of 500 – 0.001 Hz. A remote reference site was located at a distance of over 100 km of the study area. Amplitude and phase sounding curves, and impedance-tensor skew and polar diagrams were results of data processing. As it was mentioned before, a series of magnetotelluric soundings was made

along one profile with a measurement step of 1500 m. To eliminate the effects of near-surface non-homogeneities, a short continuous profiling was made instead of a single sounding (Stefaniuk 2003). The magnetotelluric continuous profiling was made along the second profile. The recorded time series were processed with the use of standard remote reference and robust data processing procedures.

#### **GEOPHYSICAL DATA INTERPRETATION**

There were two stages of the quantitative interpretation. At the first stage, the analysis of so-called parametric soundings located near deep boreholes was made. As a result, 1D models of resistivity distribution were obtained and sensitivity study was made. The models obtained for boreholes were used as starting models for 1D sounding inversion. Depths of selected seismic horizons with relatively high reliability were stabilized during the inversion. At the second stage, 2D automatic inversion was applied. For the continuous profile, 2d inversion was preceded by computation of EMAP pseudo 2D section. The NLCG algorithm was used to the first general evaluation of 2D resistivity distribution. Then, the SBI algorithm was applied to the inversion constrained by borehole and seismic data. Since the results of SBI inversion were found reliable for the basement structure while the obtained resistivity distribution of the flysch cover was rather unrealistic, the obtained basement model was stabilized and the NLCG inversion was made for the upper part of the section.

#### **GEOLOGICAL INTERPRETATION**

As a result of magnetotelluric data interpretation, the resistivity differentiation of the basement rocks due to tectonic zones and lithology changes was evaluated. The highest resistivity was probably connected with the crystalline Precambrian rocks overlain by relatively low-resistivity clastic measures of Lower Paleozoic and high-resistivity siliciclastic and carbonate sediments of Upper Paleozoic and Mesozoic. Miocene sediments have low resistivity. The boundary between Miocene complex and the flysch cover is not clear because of low-resistivity rocks building the lower part of the Carpathian overthrust in the study area. Resistivity of the upper part of the overthrust built of sandstone layers interbedded with low-resistivity shales is relatively high.

### CONCLUSIONS

The relatively detailed interpretation of the geological structure from MT soundings is possible when the external constraints are applied based on borehole and well-logging data.

2D inversion with the use of SBI code is reliable for more or less horizontally-layered geological medium. Lateral non-homogeneities in resistivity distribution are better reflected by inversion with the use of NLCCG code.

**Acknowledgements.** *This work was supported by grant from the Ministry of Scientific Research and Information Technology under contract no 5T12B 041 25. The magnetotelluric data were acquired by the Geophysical Exploration Company, partly for the Polish Oil and Gas Company. The access to other geophysical and geological data was rendered by the Polish Oil and Gas Company. MT data processing and*

*interpretation was made with the use of EMI and WinGLink Geosystem software packages, which were provided free of charge by the Geophysical Exploration Company. The authors thank the managements of those companies for the access to data and software.*

### REFERENCES

Górecki W., Stefaniuk M., Maćkowski T., Reicher B., Sliz K. K, Maksym A., Siupik J., (2004) - Joint interpretation of seismic and MT data beneath the Polish Carpathians overthrust, 66th EAGE (European Association of Geoscientists & Engineers) conference & exhibition : 7–10 June 2004, Paris : extended abstracts & exhibitors' catalogue. S. 1–4, P325.

Stefaniuk M., (2003) – Regionalne badania magnetotelluryczne w polskich Karpatach wschodnich. Zeszyty Naukowe AGH, Geologia, 3-4, 131-168.

Stefaniuk M., Maksym A., Florek R., Wojdyła M., (2005) – Magnetotelluric continuous profiling in recognition of geological structure and lithology differentiation; case studies from Polish Outer Carpathians, EGU (European Geosciences Union) General Assembly, Vienna, 2005, Geophysical Research Abstracts, vol. 7, 09251, 1 – 6.

Stefaniuk M., Wojdyła M., Czerwiński T., Maksym A., (2004) - Magnetotelluric method in hydrocarbon prospecting : case study from the Polish Carpathians, 66th EAGE [European Association of Geoscientists & Engineers] conference & exhibition : 7–10 June 2004, Paris : extended abstracts & exhibitors' catalogue S. 1–4, P323.